Crustal and uppermost mantle structure variation beneath La Réunion hotspot track

Fabrice R. R. Fontaine, Guilhem Barruol, Hrvoje Tkalcic, Ingo Wölbern, Georg Rümpker, Thomas Bodin, Méric Haugmard

Geophysical Journal International

Geophys. J. Int. (2015) **203,** 107–126
GJI Seismology

doi: 10.1093/gji/ggv279

Crustal and uppermost mantle structure variation beneath La Réunion hotspot track

Fabrice R. Fontaine,[1] Guilhem Barruol,[1] Hrvoje Tkalčić,[2] Ingo Wölbern,[3] Georg Rümpker,[3] Thomas Bodin[4,5] and Méric Haugmard[6]

[1] *Laboratoire GéoSciences Réunion, Université de La Réunion, Institut de Physique du Globe de Paris, Sorbonne Paris Cité, UMR CNRS* 7154, *Université Paris Diderot, F-*97744 *Saint Denis, France. E-mail: fabrice.fontaine@univ-reunion.fr*
[2] *Research School of Earth Sciences, The Australian National University, Canberra, ACT* 2601, *Australia*
[3] *Institute of Geosciences, Goethe-University Frankfurt, Altenhöferallee* 1, *DE-*60438 *Frankfurt am Main*
[4] *Berkeley Seimological Laboratory,* 215 *McCone Hall, UC Berkeley, Berkeley CA* 94720–4760, *USA*
[5] *Laboratoire de Géologie de Lyon, Ecole Normale Supérieure de Lyon, Université de Lyon-*1, *CNRS, F-*69364 *Lyon Cedex* 07, *France*
[6] *Laboratoire de Planétologie et Géodynamique, Université de Nantes, UMR-CNRS* 6112, *F-*44322 *Nantes Cedex* 3, *France*

Accepted 2015 June 26. Received 2015 May 16; in original form 2015 February 3

SUMMARY

The Piton de la Fournaise basaltic volcano, on La Réunion Island in the western Indian Ocean, is one of the most active volcanoes in the world. This volcano is classically considered as the surface expression of an upwelling mantle plume and its activity is continuously monitored, providing detailed information on its superficial dynamics and on the edifice structure. Deeper crustal and upper mantle structure under La Réunion Island is surprisingly poorly constrained, motivating this study. We used receiver function techniques to determine a shear wave velocity profile through the crust and uppermost mantle beneath La Réunion, but also at other seismic stations located on the hotspot track, to investigate the plume and lithosphere interaction and its evolution through time. Receiver functions (RFs) were computed at permanent broad-band seismic stations from the GEOSCOPE network (on La Réunion and Rodrigues), at IRIS stations MRIV and DGAR installed on Mauritius and Diego Garcia islands, and at the GEOFON stations KAAM and HMDM on the Maldives. We performed non-linear inversions of RFs through modelling of *P*-to-*S* conversions at various crustal and upper mantle interfaces. Joint inversion of RF and surface wave dispersion data suggests a much deeper Mohorovičić discontinuity (Moho) beneath Mauritius (∼21 km) compared to La Réunion (∼12 km). A magmatic underplated body may be present under La Réunion as a thin layer (≤3 km thick), as suggested by a previous seismic refraction study, and as a much thicker layer beneath other stations located on the hotspot track, suggesting that underplating is an important process resulting from the plume–lithosphere interaction. We find evidence for a strikingly low velocity layer starting at about 33 km depth beneath La Réunion that we interpret as a zone of partial melt beneath the active volcano. We finally observe low velocities below 70 km beneath La Réunion and below 50 km beneath Mauritius that could represent the base of the oceanic lithosphere.

Key words: Surface waves and free oscillations; Oceanic hotspots and intraplate volcanism; Hotspots; Crustal structure; Indian Ocean.

1 INTRODUCTION

1.1 Deccan-Réunion mantle plume

La Réunion hotspot has been proposed to represent the present-day surface expression of a deep mantle plume upwelling (e.g. Morgan 1971; Courtillot *et al.* 2003), with a possible source in the lower mantle at depth ≥1900 km (Montelli *et al.* 2004). Even though the structure of the volcanic edifice has been investigated by numerous studies (e.g. Nercessian *et al.* 1996; Brenguier *et al.* 2007; Prôno *et al.* 2009), our knowledge on the deeper crust and mantle structure is poor due to limited instrumental coverage. Crustal structure beneath La Réunion Island was primarily deduced from seismic refraction profiles that suggested the presence of an underplated magmatic body at the base of the oceanic crust up to 3 km thick (Charvis *et al.* 1999; Gallart *et al.* 1999). At larger scale and

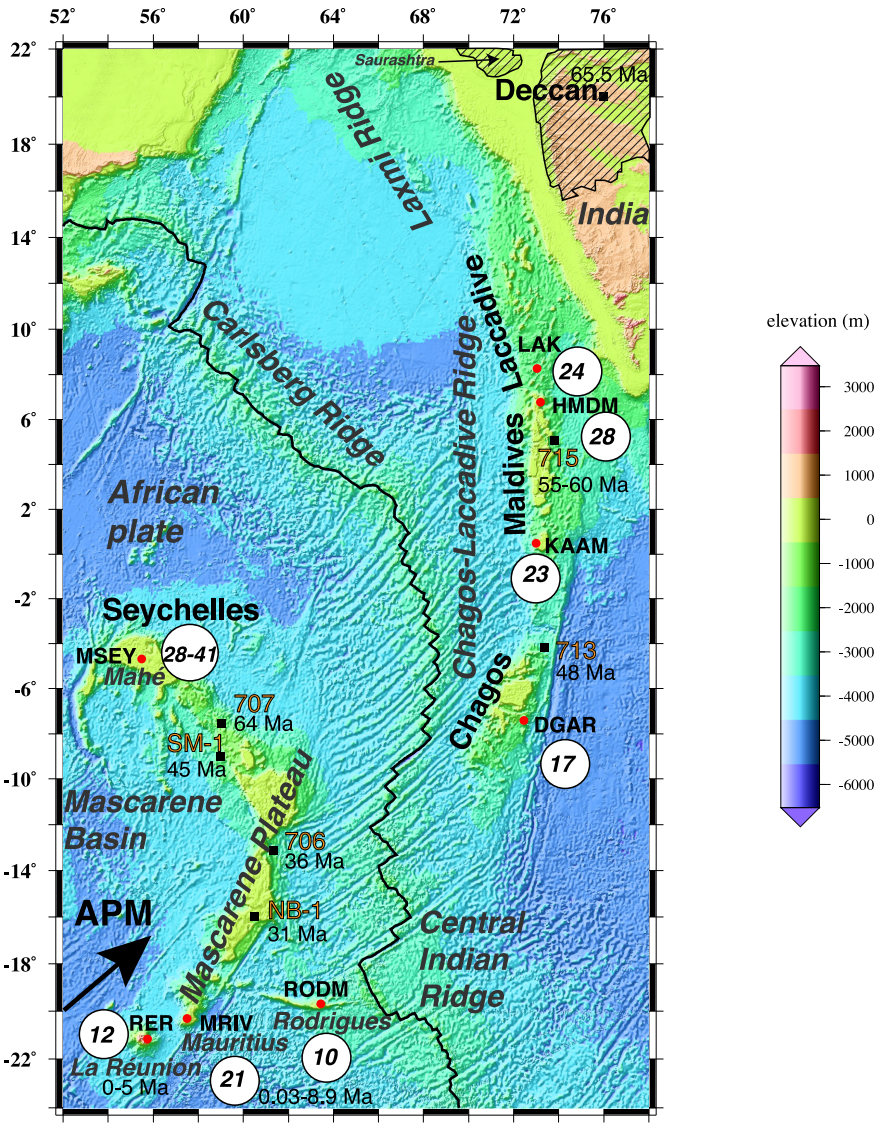

Figure 1. Bathymetric and topographic map of the studied area (e.g. Smith & Sandwell 1997). The Moho depths calculated from this study are indicated in the white circles together with the previous crustal thickness estimates from receiver function analysis at Minicoy Island (Gupta *et al.* 2010) and Seychelles Plateau (Hammond *et al.* 2012, 2013). MSEY is a permanent station installed on the island of Mahé and LAK shows the location of two temporary seismometers (~200 m apart) at Minicoy Island (Lakshadweep). The hatched domain represents the Deccan volcanic province. The crustal ages estimated at Leg 115 drilling sites 706, 707, 713 and 715 (Duncan 1990; Duncan & Hargraves 1990) are shown. NB-1, Nazareth Bank and SM-1, Saya de Malha industrial wells (O'Neill *et al.* 2005). APM is the present-day absolute plate motion from the HS2-NUVEL1A model from Gripp & Gordon (1990).

depths, the modifications induced by the Réunion plume to the Indo-Australian and African lithospheres are still unclear. Through this work, we therefore aim at constraining features beneath the hotspot track such as the crustal structure, the thermomechanical thinning of the lithosphere, the presence of partial melt and the proportion of plume material possibly intruded at depth.

The Deccan Traps dated at about 65–66 Ma (e.g. Courtillot *et al.* 1986) represent a large volcanic igneous province covering about 500 000 km^2 of India (Fig. 1) and is assumed to be the first signature of the Réunion plume, also present on Praslin Island (Devey & Stephens 1991) located at around 40 km northeast of Mahé Island in the Seychelles (Fig. 1). Despite the age progression from the Deccan to La Réunion Island as reported Fig. 1 (Duncan 1990; Duncan & Hargraves 1990), the link between the Deccan Traps and the Réunion hotspot is not always accepted (e.g. Burke 1996; Sheth 1999). In the classical scenario, the Deccan Traps was formed from a plume head impact. The subsequent northward motion of India relative to the upwelling plume induced the Chagos-Laccadive Ridge on the Indian plate. Since 34 Ma, the African Plate moved northeastward and the hotspot activity constructed successively the Mascarene Plateau, Mauritius and La Réunion (Duncan 1990). The Indian lithosphere was moving rapidly northward from Cretaceous until early Oligocene (Duncan 1981). Based on a slow motion of the African Plate relative to the asthenosphere since 30 Ma, Burke (1996) proposed that La Réunion, Mauritius and Rodrigues islands could have been generated from younger hotspots than the Deccan plume.

Volcanic activity on Mauritius is estimated to start earlier than 8.9 Ma, which is the age of the oldest rocks dated for the emerged part of the island and occurred until 0.03 Ma (Moore *et al.* 2011). Rodrigues Island, dated at 1.5 Ma (McDougall *et al.* 1965), is not located on the hotspot track, but on the Rodrigues Ridge (Fig. 2a), an

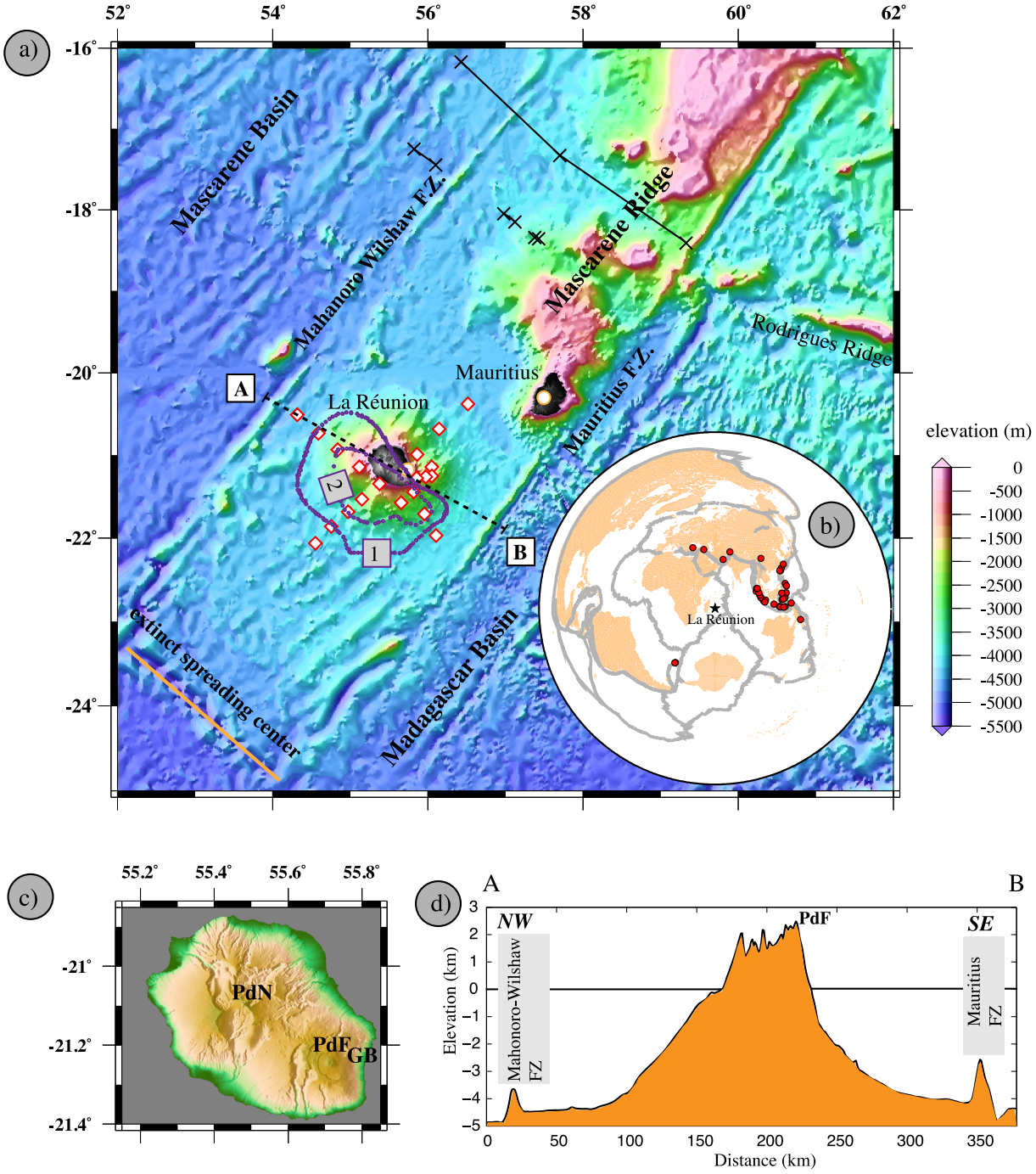

Figure 2. (a) Relief map of La Réunion area with location of two fracture zones. We used topography data from Smith & Sandwell (1997). The orange circles show the location of RER permanent GEOSCOPE seismic station on the Piton de la Fournaise volcano and MRIV permanent IRIS station on Mauritius. Isocontours of the thickness of underplated magmatic body beneath La Réunion are indicated in purple and issued from wide-angle seismic lines shot from two previous studies (Charvis *et al.* 1999; Gallart *et al.* 1999). Red diamonds near La Réunion show the location of OBS used during these two studies. The black stars indicate locations of heat flow measurements realized across the Mascarene Ridge from two profiles (Bonneville *et al.* 1995, 1997). (b) Location map of events (in red) producing radial RFs with a signal to noise ratio ≥2 at RER station (black star). (c) Topographic map of La Réunion Island. PdN: Piton des Neiges, PdF, Piton de la Fournaise and GB, Grand Brûlé. (d) NW–SE topographic profile across La Réunion Island along the AB profile. The topography suggests a transition between the volcanic edifice and the oceanic crust between 4 and 5 km depth below the sea level.

east–west volcanic lineament formed between 7 and 10 Ma (Dyment *et al.* 2007). The Rodrigues Ridge has been proposed to result from a ridge—hotspot interaction (Morgan 1978) and could represent the surface expression of a channelled asthenospheric flow connecting La Réunion hotspot and the ridge axis, on which one retrieves geochemical signatures from La Réunion hotspot (e.g. Füri *et al.* 2011). First eruptions forming La Réunion Island (Figs 2b and c) are estimated to be around 5 Ma (e.g. Gillot *et al.* 1994) or even older, around 7 Ma (Lénat *et al.* 2001). The present-day volcanic activity on the hotspot track is located on the Piton de la Fournaise volcano (Figs 2c and d), which is active since *ca.* 530 ka (Gillot & Nativel 1989) and that succeeded to the activity of the Piton

des Neiges volcano with a subaerial activity from *ca*. 2.1 Ma to 12 ka (McDougall 1971; Deniel *et al.* 1992). An ancient volcano underlying the Piton de la Fournaise was proposed by Malengreau *et al.* (1999) based on gravimetric anomalies and by a gabbroic and cumulate complex identified between 1 and 3 km below sea level (bsl) with deep geothermal exploration drill hole in the Grand Brûlé area (Fig. 2c), in the eastern part of the island (Rançon *et al.* 1989). The dormant and active volcanoes on La Réunion are aligned along an overall N120°–130° direction, that is roughly perpendicular to the present-day absolute plate motion (APM) of the African Plate near La Réunion, which is 26 mm yr^{-1} along the direction N50°E (as in HS2-NUVEL1A model from Gripp & Gordon 1990). This also suggests an important crustal and lithospheric control on the volcanic activity (Michon *et al.* 2007; Bissessur 2011).

1.2 Receiver function methods

In order to characterize the plume influence on the lithosphere thinning, on the crustal thickness, and on possible underplating processes that might occur, we investigate in this study the crustal and uppermost mantle structure but also beneath several areas along La Réunion hotspot track using teleseismic receiver functions (RFs). Various state-of-the-art methods and inversion techniques are applied to data recorded by permanent seismic stations installed on the islands located on or near the hotspot track from La Réunion to the Maldives. The coda of teleseismic *P* waves contains considerable information about the structure of the Earth directly beneath a seismic station. The *P*-receiver function technique isolates *P*-to-*S* conversions generated at crustal and upper mantle discontinuities beneath the recording site (e.g. Phinney 1964; Burdick & Langston 1977; Langston 1977, 1979; Vinnik 1977) by source equalization. Conversion primarily occurs at the Moho, which represents one of the most significant interfaces (taking into account the possible presence of sedimentary layers beneath some seismic stations) in terms of the variations in density and elastic properties. The principle underlying the RFs technique is to extract the structure underlying the station by removing the instrument response and the effect of passage through the bulk of the mantle through deconvolution of different components of ground motion. RFs are sensitive to shear wave velocity (v_S) contrasts of interfaces located beneath the seismic station. However, they are only weakly sensitive to absolute velocities (e.g. Juliá *et al.* 2000) and hence the *S*-velocity structure is better resolved with a joint inversion of radial RFs and surface wave dispersion (SWD) data (e.g. Özalaybey *et al.* 1997; Du & Foulger 1999; Tkalčić *et al.* 2006, 2012). In this study, we use the radial RFs, obtained by deconvolving the radial component (along the great-circle to the source) by the vertical component, as a means of investigating the depth of physical interfaces beneath the permanent seismic stations located on La Réunion hotspot track. We produce a map of the crustal thickness and we estimate the depth of the lithosphere beneath La Réunion, Mauritius and Rodrigues. This work also allows us to study the nature of the crust–mantle transition, and to detect the presence of partial melt or subcrustal, underplated material.

2 DATA

Receiver functions were determined at the permanent broad-band seismic stations located on or in the vicinity of the Réunion plume track. We analysed ∼20 yr of data at RER permanent seismic station (from 1994 to 2013). This broad-band seismic station is one of the first station installed by the GEOSCOPE French global seismic network. At the other stations, the data availability is smaller due to their more recent installation. We processed ∼4 yr at MRIV (2010–2013), 2.5 yr of data (2011–2013/06) for stations on Rodrigues (RODM and ROCAM), 9 yr at DGAR (2004–2012) and 5 yr (2008–2012) at stations from the GEOFON German global network of broad-band seismic stations (HMDM and KAAM).

Due to the proximity to the ocean, the quality of the seismic data is not as high as in quiet continental areas and makes receiver functions more difficult to obtain. These island stations have higher level of noise than continental stations (located more than 150 km to the coast) as shown by Stutzmann *et al.* (2000) for RER station. A high noise level reduces the number of receiver functions that can be measured at each station as seismograms with seismic noise level on the radial component close to the amplitude of the direct *P* phase are rejected in order to successfully isolate the direct *P* phase and the Moho-converted *Pms* phase. Furthermore, the level of data noise controls the information that an inversion of RF could obtain from the data, that is, how well the model can be resolved (e.g. Bodin *et al.* 2012a). The Transdimensional Bayesian inversion that we use in this work allows us to consider both the level of data noise and complexity of the model (i.e. number of layers) as unknowns in the problem.

3 RF OBSERVATIONS

We used five permanent seismic stations installed on the La Réunion hotspot track and two stations on Rodrigues. We analyse *P* waves from epicentral distances between 30° and 90° for events with $m_b \geq 6.0$ (as shown Fig. 2b for station RER), hand-selected for high signal-to-noise ratio (SNR ≥ 2). We cut the seismic traces 5 s prior to and 30 s after the initial *P*-wave arrival. A Gaussian low-pass filter with a width *a* of 2.5 rad s^{-1} (which correspond to a low-pass filter with a corner frequency of ∼1.2 Hz) is applied to the waveforms before the deconvolution is performed to eliminate high frequencies stemming from the ambient noise and small-scale crustal heterogeneities. The *P* radial RFs are obtained by deconvolving the radial component, directed along the great circle between source and receiver, with the vertical component in the time domain (Ligorria & Ammon 1999). The RF waveform is sampled at a frequency of 10 Hz. The radial RFs at each seismic station were then stacked for a set of backazimuths, with a narrow range of ray-parameters based on the following procedure (Fontaine *et al.* 2013a,b):

(1) Select the quadrant (backazimuths between N0°–N90°, N90°–N180°, N180°–N270°, N270°–N360°) with the highest number of RFs.

(2) Compute p_{median}: the median of the ray parameters corresponding to all seismic events in this interval.

(3) Select events with a ray parameter $= p_{median} \pm 0.006$ s km^{-1}. From our experience (e.g. Fontaine *et al.* 2013a; Lamarque *et al.* 2015), this range of ray parameters is still narrow enough that RFs do not require corrections of converted phases (i.e. moveout corrections), given the depth range investigated. Most data come from seismogenic belts surrounding Indonesia and along the Philippine trench (Fig. 2b), and this narrows down the range of ray parameters that we can utilize in the processing of RFs. For example, the useful ray parameter range for station RER is between 0.050 and 0.062 s km^{-1}.

(4) Stack the RFs selected in the previous step. Only mutually coherent RFs are used for stacking and we focus on obtaining the

most basic information assuming a horizontally layered structure without anisotropy. The stacking process may induce a loss of some features of the crust–mantle boundary particularly associated with the detection of dipping and anisotropic structures that depend on the backazimuthal variation of the RF amplitude. However, the goal of this study and particularly with the present limited backazimuthal coverage is not to constrain dipping effect or anisotropic effect on the RFs (e.g. Peng & Humphreys 1997; Savage 1998; Fontaine *et al.* 2013b). Instead, we choose to concentrate on stacking similar radial RFs for a limited range of backazimuths and ray parameters in order to estimate the depths of first-order seismic discontinuities present beneath the station (e.g. Fontaine *et al.* 2013a; Lamarque *et al.* 2015). Before each stack, we examine the coherency of individual RFs using the cross-correlation matrix approach from Tkalčić *et al.* (2011): we compute the cross-correlation coefficients for each pair of RFs. Then individual RFs are selected or rejected using empirical values for the minimum coefficient of cross-correlation χ and the percentage of coherent RFs τ. More specifically, a single RF is selected for stacking and deemed mutually coherent with other selected RFs if it cross-correlates with at least τ per cent of other RFs with the cross-correlation coefficient at least equal to χ. In this study, for most stations, relatively small numbers of RFs (<50) result in the choice of $\chi = 0.70$, and τ between 4 per cent for DGAR and 22 per cent for RODM. We show in the electronic supplement (Appendix A1a and Appendix A2a) the individual RFs traces obtained at each seismic station and the resulting stack used in the inversions.

In the RF inversions, we cut the traces 12 s after the direct *P* wave arrival time, whereas the signal was cut after 17 s for the joint inversions.

4 INVERSION OF RECEIVER FUNCTIONS

We perform two different non-linear inversions of RFs: first with the widely used Neighbourhood Algorithm (e.g. Sambridge 1999a,b) and second with the recently applied Transdimensional Bayesian approach (Bodin *et al.* 2012a). Since these methods require testing a large number of models against the data, they are much more computationally expensive than conventional linearized procedures.

4.1 Neighbourhood Algorithm inversion of receiver functions

A nonlinear inversion method, the Neighbourhood Algorithm (NA, Sambridge 1999a,b) was employed to match the observed radial RFs. As for the forward problem utilized in the inversion, the synthetic radial RF is calculated using the Thomson-Haskell matrix method (Thomson 1950; Haskell 1953; Haskell 1962). The full effects of free-surface reverberations and conversions are modelled. This inversion technique samples regions of a multidimensional parameter space that have acceptable data fit (Sambridge 1999a, 2001). At each iteration, the entire parameter space is partitioned into a set of Voronoi cells (Voronoi 1908) constructed about each previously sampled model. In our case, Voronoi cells are nearest neighbour regions defined by an L_2-norm. The initial sets of samples are uniformly random, but as iterations proceed, only a subset of chosen Voronoi cells is resampled (using a random walk within each cell). This allows the NA to concentrate where data misfit is lowest. The NA requires two control parameters:

n_s, which is the number of models generated at each iteration, and

n_r which is the number of neighbourhoods resampled at each iteration.

After several trials, we empirically specify the maximum number of iterations to 1800, $n_s = 200$ for the first iteration, $n_s = 25$ for all other iterations and $n_r = 25$ for all iterations. The *a priori* distribution of the misfit function is assumed to be Gaussian (e.g. Sambridge 1999a, 2001). In this study, we used a χ^2 metric similar to that employed by Sambridge (2001) to compute the misfit function. The misfit function, a L_2-norm, is defined as the sum of the squares of the difference between the observed amplitude of the radial RF and the amplitude of the synthetic radial RF from a 5-layer model. Fontaine *et al.* (2013a) show an example of the misfit function obtained using the NA (their fig. 3a).

The NA inversion provides a set of best-fitting 1-D shear wave velocity models and an estimate of the v_P/v_S. However, neither the v_P/v_S ratios nor the absolute velocities are strongly constrained in the NA inversion, which is most sensitive to the depth of discontinuities. We characterize the crust and uppermost mantle structure with a 5-layer 1-D seismic velocity model and the bounds of the 20 parameters are specified in Appendix B. The NA method combines a Monte Carlo search technique and the properties of the Voronoi geometry in parameter space to find an ensemble of the best fitting models and performs a global optimization. One of the advantages of the NA over other direct search methods is that only the rank of models with respect to the misfit function is used to compare models and this enhances the exploration of parameter space to find suitable models. The NA algorithm quickly converges toward an ensemble solution (e.g. Sambridge 1999a; Fontaine *et al.* 2013a). Therefore, we consider an ensemble of the best 1000 data fitting *S*-velocity models generated by the NA at each station. The average of the best 1000 models is used to estimate the structure beneath each seismic station. Sambridge (1999b) used a Bayesian approach to estimate resolution and confidence intervals of all the parameters in the RF inversion. The layer thickness distribution and the *S*-velocity distribution are better constrained by the NA inversion than the v_P/v_S ratio, thus we place less reliance on the v_P/v_S ratio. Sambridge (1999b) showed using marginal probability density functions that the v_P/v_S ratio from the NA inversion is better resolved in the first layer and poorly resolved in the remaining layers. The inclusion of the v_P/v_S ratio serves primarily to allow for some of the effects of the sedimentary layer beneath the stations with no *a priori* information (Bannister *et al.* 2003).

4.2 Transdimensional Bayesian (TB) inversion of receiver functions

Transdimensional inference (where the dimension of the model is variable) has been recently introduced and applied to a wide range of problems in Earth sciences (e.g. Malinverno 2002; Sambridge *et al.* 2006; Hopcroft *et al.* 2009; Dettmer *et al.* 2010; Piana Agostinetti & Malinverno 2010; Gallagher *et al.* 2011; Bodin *et al.* 2012a,b; Iaffaldano *et al.* 2012). TB inversion of RFs is a fully non-linear inversion approach cast in a Bayesian (i.e. probabilistic) framework (e.g. Green 2003; Sambridge *et al.* 2006; Bodin *et al.* 2012a). It presents two advantages in comparison with the NA inversion: (1) The complexity of the imaged structure (the number of layers) can be treated as unknown in the inversion, which adapts to the level of information present in the data through the principle knows as 'natural parsimony' (Malinverno 2002). (2) The solution is

probabilistic, which enables rigorous quantification of uncertainties and trade-offs.

Similarly to the NA approach, the average receiver function can be inverted for a 1-D profile of shear wave velocity under the station. Here, the solution is a probability distribution of model parameters that fully accounts for the non-uniqueness of the problem. This target distribution is defined through Bayes' theorem as the probability density of the model parameters given the observed data, namely the posterior distribution (Bayes 1763).

Here we sample the posterior probability function (Appendix C) with the reversible jump Markov chain Monte Carlo algorithm (rj-McMC; Green 1995, 2003), as implemented in Bodin *et al.* (2012a). At each step of the Markov chain, a model is proposed and either 'accepted' or 'rejected' in the ensemble solution. The first part of the chain of sampled model is discarded. After this 'burn-in' period, the random walk is assumed to be stationary and starts to produce a type of 'importance sampling' of the model space. That is, the sampled models are asymptotically distributed according to the posterior distribution, and can be used to describe the state of knowledge we have about the Earth. For example, a solution model and its uncertainties can be calculated from the mean and variance of the ensemble solution.

The reversible jump algorithm was run on 32 parallel cpu-cores sampling the model space simultaneously and independently. Each chain was run for 1.6×10^6 steps. The first 8×10^5 models were discarded as burn-in steps and after this burn-in period the sampling algorithm showed a convergence. Then, each 100th model visited was selected for the ensemble to eliminate dependent samples in the ensemble. We also invert for the number of layers and the level of data noise. The noise is assumed to be correlated and we used a Gaussian correlation function to model RF uncertainties (Bodin *et al.* 2012a). The transdimensional sampling was run for a number of layers varying between 3 and 24. Bounds for the uniform prior distribution were set to 1.5–5.5 km s^{-1} for *S*-wave velocity values. For more details about TB inversion of RFs, we refer the reader to Bodin *et al.* (2012a).

4.3 Transdimensional joint inversion of receiver function and surface wave dispersion data

RFs and SWD have complementary sensitivities. While RFs are particularly suited to constrain the depth of seismic discontinuities, they are only sensitive to discontinuous changes in *S*-wave velocities in different layers. Conversely, SWD curves are sensitive to absolute *S*-wave velocities and are poor in locating the depth of seismic discontinuities (e.g. Juliá *et al.* 2000). Joint inversion of RF and SWD data is therefore expected to bring significantly better-resolved velocity models.

The spatial resolution of Rayleigh wave at 20 mHz (50 s period) is in general low in the Indian Ocean (Ma *et al.* 2014). For RER and MRIV stations for which the resolution of the LITHO1.0 model is better than at the other seismic stations, we conducted a joint inversion of RF and SWD measurements. The RF waveform was sampled at a frequency of 6.25 Hz giving a total of 139 data samples. We extracted Rayleigh wave group velocity dispersion data from the LITHO1.0 model (Ma *et al.* 2014; Pasyanos *et al.* 2014) for periods between 25 and 100 s. The long period dispersion measurements allow us to invert down to ∼125 km depth.

The joint inversion technique within the Bayesian transdimensional hierarchical framework is based on the same principles presented above for the inversion of RFs only (see Bodin *et al.* 2012a for details).

5 RESULTS

Results issued from NA and TB inversions of RF show similar general trends at all seismic stations. TB inversion allows higher resolution of velocity variation as models with higher number of layers are recovered from the inversion. TB inversion of RF has not yet been tested on the field data, apart from an example station in Bodin *et al.* (2012a).

We performed synthetic RF computation and inversion for 5-layer models including an underplated layer. We use the synthetic seismogram algorithm of Randall (1989) based on the reflection-matrix method developed by Kennett (1983) and a time domain deconvolution (Ligorria & Ammon 1999) to compute the synthetic RF. The inversions show that due to the frequency range used in this RF analysis we do not have the resolution to detect an underplated layer of thickness <2 km. The uncertainty of the Moho depth measurements is around 2 km similar to that observed in previous studies (e.g. Fontaine *et al.* 2013a).

La Réunion. A peak on the radial component of the RFs is observed at ∼1.1 s after the direct *P* phase (Figs 3a & b and Appendix A1a). This phase corresponds to the *Pms* phase. The nature of this seismic phase recorded at RER but also at the other stations described below were confirmed by simple calculations and by synthetic RFs generated from models including up to 5 layers, both showing that the peak at ∼1.1 s represents the *Pms* phase. A sharp increase of velocity is observed at 4 km below sea level from RF inversions (Figs 3c and d) and may correspond to the transition between the volcanic edifice and the oceanic crust. Moho depth estimated from RF inversion with the transdimensional method (Fig. 3d) is at ∼12 km bsl beneath RER (i.e. ∼13 km below the Earth's surface). A low velocity zone is observed beneath ∼28 km bsl from the transdimensional inversion (Fig. 3d). The results of joint inversion of SWD (Fig. 4a) and RF data (Fig. 4b) show a sharp decrease of the velocity between 0 and ∼1 km bsl (Figs 4c and d). A LVZ is observed between 2 and 3 km bsl. A sharp increase of velocity is also observed at 4 km. Then, the shear wave speed increases down to ∼10 km depth and from 10 to 12 km it is increasing gradually up to 4.4 km s^{-1}. This result suggests a relatively thin crust-mantle transition. The velocity then keeps increasing until a depth of 19 km. A sharp negative velocity jump is observed at a depth of about 33 km bsl, ∼5 km deeper than determined from the inversion of the RF alone but very likely corresponds to the same structure and could indicate both the presence of partial melt and/or high temperature (as discussed in Section 6.4). A seismic discontinuity is also suggested at ∼70 km bsl, where the average velocity gradually decreases (Fig. 4d), which may correspond to the large-scale lithosphere–asthenosphere boundary (LAB) beneath this region, as discussed later.

Mauritius. The average of radial RFs exhibits a peak around 2 s after the direct *P* phase (Figs 5a & b and Appendix A1b). Results from NA and TB inversions (Figs 5c and d) show a sharp increase of the average shear wave speed from 0 to 2 km bsl and followed by a slight increase of the velocity between ∼2 and 14 km. The velocity jump observed at 14 km depth is compatible with results from H–κ stacking (Appendix D) and also from the joint inversion. The velocity then increases gradually down to a depth of 21 km (Figs 5c and d), the boundary we consider to represent the Moho.

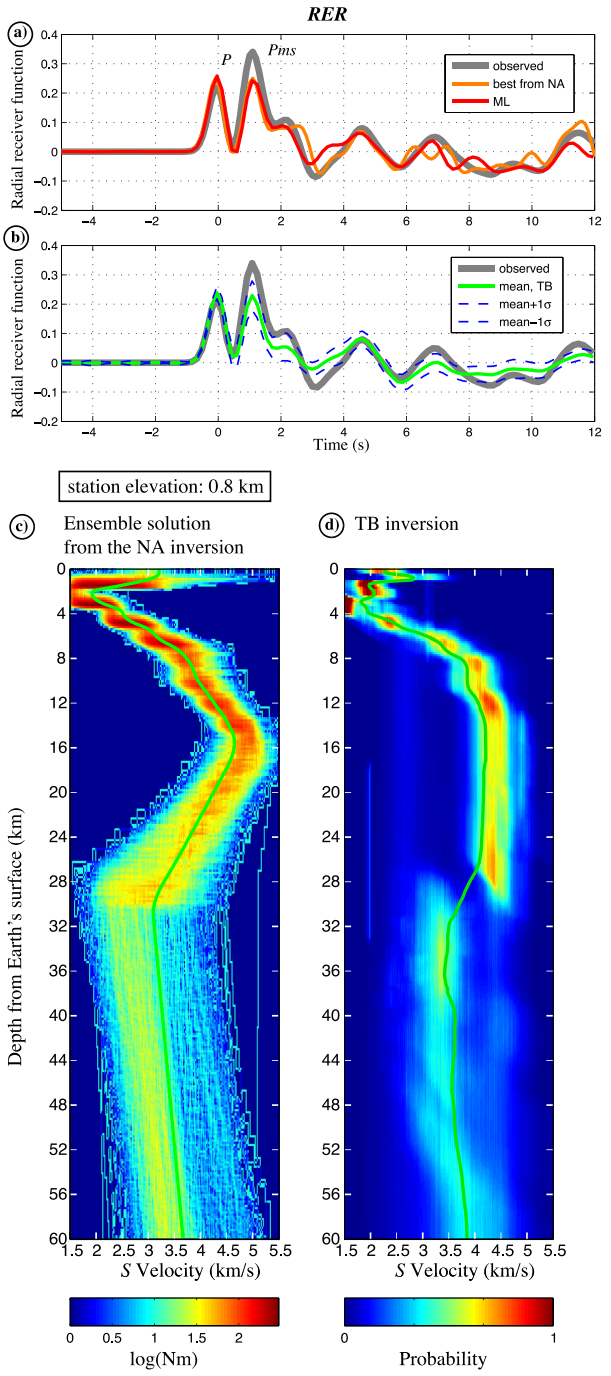

Figure 3. Receiver functions and inversions performed at station RER: (a) comparison between the observed average (in grey) and the predicted radial RFs from the best fitting model resulting from the NA inversion (in orange) and the transdimensional inversion (in red) at RER. ML is for 'maximum likelihood' and is obtained from the first cpu-core. (b) Comparison between the observed average (in grey) of RFs and the average RF (in green) from the transdimensional inversion representing the average RF of all RFs predicted for the ensemble of (800 000) models sampled during the post burn-in period. Dashed blue lines represent ±1 standard deviation bounds around the average. (c) Best 1000 models from 45 200 models issued from the NA inversion, shown in blue, yellow and red, with the colour being logarithmically proportional to number of models. The colour scale shows the increase in data fit from blue to red. A solid green line shows the average model of the best 1000 fitting models. (d) Posterior probability distribution for v_S at each depth determined from the TB inversion. The green curve represents the average solution model.

A sharp negative velocity jump is observed below ∼50 km depth (Fig. 5d) and may correspond to the LAB.

The joint inversion of SWD (Fig. 6a) and RF data (Fig. 6b) at MRIV results in a sharp velocity increase down to a depth of about 2 km bsl (Figs 6c and d). A seismic discontinuity is observed at *ca.* 4 km bsl. From 6 to 16 km, the velocity keeps increasing slightly. A stronger increase is observed between 16 and *ca.* 21 km (Figs 6c and d). v_S increases from 4 to ∼4.4 km s^{-1}. Then, small variations confined between ∼4.5 and ∼4.6 km s^{-1} are observed to the depth of 50 km. Below 50 km, a sharp negative jump is observed. If one assumes that this represents the base of the lithosphere, MRIV could be characterized by a thinner lithospheric mantle lid than RER.

Rodrigues. The first phase visible on the averaged radial RF corresponds to a smaller peak than the second phase (Figs 7a & b and Appendix A2a) as observed at RER station. This latter phase arrives around 1 s after the first phase and corresponds to the *Pms* phase. The smaller amplitude first peak may be due to a low-velocity layer just below the Earth's surface as observed by 1-D RFs modelling (Zelt & Ellis 1999) and also shown by the ensemble solution from the inversions (Fig. 7c). The Moho depth is estimated at 10 km and the crust–mantle transition is sharper than at other stations (Fig. 7d). A low velocity zone (LVZ) is observed between 25 and 40 km bsl (Fig. 7d) and likely corresponds to the asthenosphere at this station, which is located above a rather young—and therefore thin—lithosphere (∼13 Ma).

Diego Garcia atoll (Chagos). On most individual radial RFs two peaks are observed before 1.4 s, one for the direct *P* wave and one for a phase at 1.3 s (Appendix A2b). After stacking, a single peak is clearly appearing with a little bump at 1.3 s (Figs 8a & b and Appendix A2b). Lateral variability beneath DGAR station may explain the fact that the stack results in one single peak instead of two. The little bump at 1.3 s may correspond to a discontinuity at around 12 km depth as suggested by both NA and TB inversions (Figs 8c and d). On an average profile (Fig. 8d) derived from the TB inversion a sharp increase is observed at around 4 km, which may correspond to the transition from the edifice to the crust. A gradual increase is observed from 14 km to *ca.* 17 km in the profile derived from the TB inversion. The Moho depth is estimated at a depth of *ca.* 17 km (Fig. 8d). We note that both at 12 and at 17 km, most velocities are compatible with velocity expected for the upper mantle.

Maldives. A broader crust–mantle transition and thicker crust than at the other stations is observed. On Huvadhu atoll (KAAM station) a first peak smaller than the second is observed on the average of radial RFs (Figs 9a & b and Appendix A2c). The first peak is also observed with a phase lag. This smaller first phase may be due to the fact that the station is installed on coral reef and such a sedimentary layer would also delay the direct *P* phase (e.g. Sheehan *et al.* 1995; Zelt & Ellis 1999). A first peak of small amplitude is expected for a thin low-velocity sedimentary layer from one-dimensional RFs modelling (Zelt & Ellis 1999). A second peak is present at around 1.3 s and may correspond to the *P*-to-*s* conversion at the former Moho discontinuity (i.e. the initial crust–mantle boundary before magmatic underplating), then a third peak at *ca.* 2.5–2.8 s representing the actual *Pms* phase, which is confirmed by RF modelling. A seismic discontinuity is suggested at 4 km depth from both NA and TB results (Figs 9c and d). TB inversions also suggest a discontinuity at ∼10 km (Fig. 9d). At greater depths, NA and TB inversion results show a discontinuity at ∼13 km. The *S* velocity is increasing from 4 to 13 km bsl (Figs 9c and d) and at 13 km v_S is between 4.4 and 4.6 km s^{-1}. Thus, this depth may represent the initial Moho depth (i.e. before the formation of magmatic

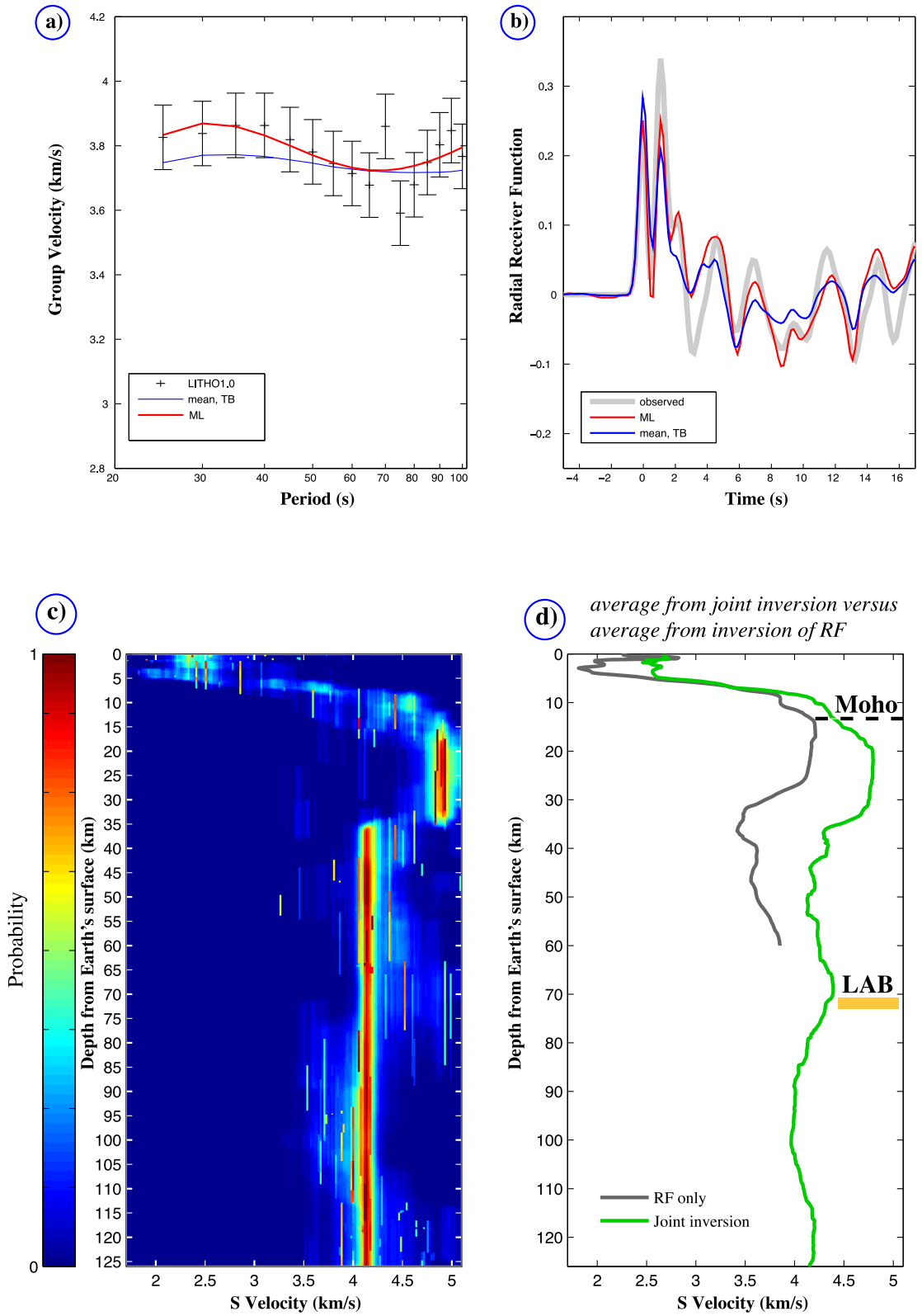

Figure 4. Results from joint inversion of RF and SWD data at RER station. (a) SWD data from LITHO1.0 model compared to predicted data for the best model (in red) and the average SWD for the ensemble of models sampled during the post burn-in period (in blue). (b) Comparison between the observed average RF (grey curve), the predicted RF from the best fitting model resulting from the transdimensional joint inversion (in red) and the average RF of the ensemble of models sampled during the post burn-in period (in blue). (c) Probability distribution for v_S at each depth. The ensemble solution, which contains 3×10^5 models, is fully represented with a colour density plot. (d) Comparison between the average solution model from the inversion of the RF (in grey) and the average solution model from the joint inversion (in green). The average solution model shows two LVZs: at about 33 and 70 km depths. LAB: possible depth of the lithosphere asthenosphere boundary.

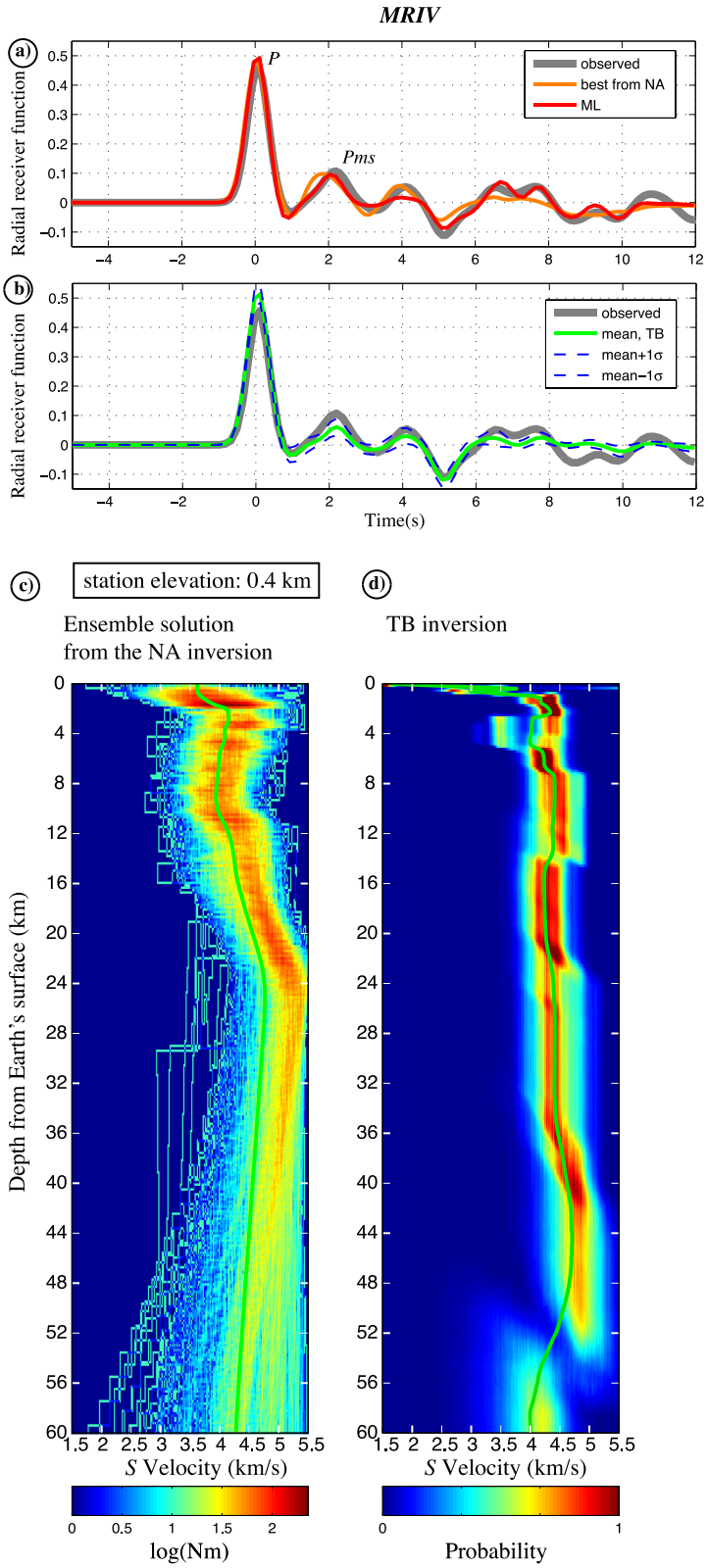

Figure 5. Receiver functions and inversions performed at station MRIV. Description as in Fig. 3.

underplated rocks). Another discontinuity is suggested at ∼23 km and it may correspond to the present Moho. Simple estimation of the differential travel time between *Pms* and *P* for a simple model with a single layer crust of 23 km thick, $v_P = 6.3$ km s^{-1}, a ray parameter of 0.0655 s km^{-1} and v_P/v_S ratio of 1.72 (using eq. 2 from Zhu & Kanamori 2000) shows that the *Pms* phase arrives around 2.8 s after the direct *P* phase. A LVZ is observed beneath station KAAM at ∼44 km depth.

On Thiladhunmathi Dhekunuburi (Haa Dhaalu atoll), the averaged radial RF of HMDM station shows a second phase following

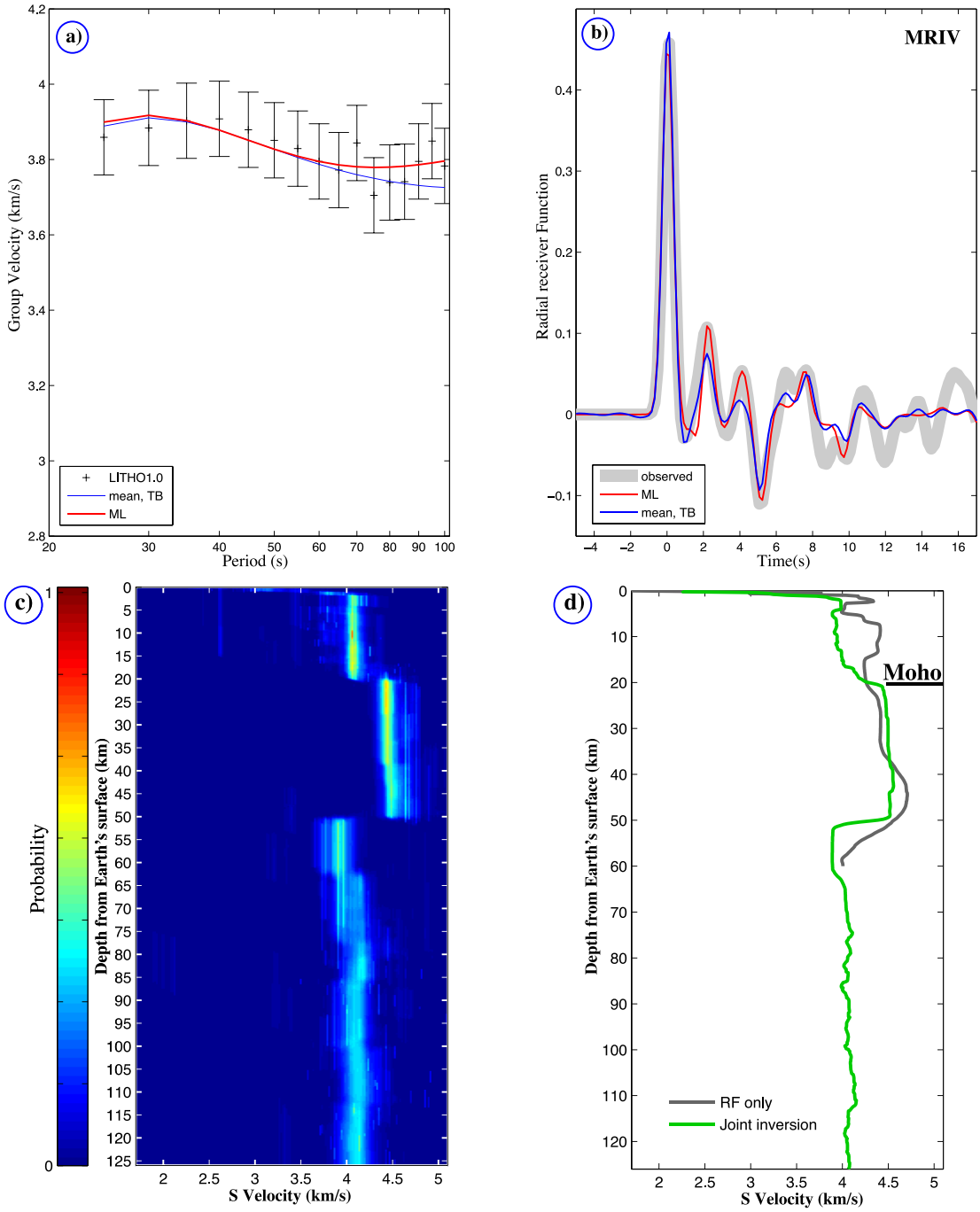

Figure 6. Joint inversion results at MRIV station. (a), (b) and (c) Description as in Figs 4(a)–(c). Excepting that the ensemble solution contains 1.6×10^5 models. (d) Comparison between the average solution model from the inversion of the RF (in grey) and the average solution model from the joint inversion (in green). A LVZ is observed at 50 km depth.

the *P*-arrival at ∼1.2 s and a third peak at ∼3.4 s (Figs 10a & b and Appendix A2d). A gradual velocity increase is observed at ∼4 km in the average velocity model from the NA and TB inversions (Figs 10c and d) up to ∼8 km. A peak in the probability of having a discontinuity is present at ∼14 km (Fig. 10d). Then the velocity increases gradually down to ∼28 km in the TB inversion, which is compatible with the NA inversion that suggests an increase from 16 to 29 km. The mean Moho depth is estimated at ∼28 km beneath HMDM based on the TB inversion. No clear LVZ is observed below this depth.

6 DISCUSSION

6.1 Comparison with previous studies

La Réunion. Li *et al.* (2003) estimated the Moho depth at 10.7 km beneath RER using RFs analysis and a transformation of the arrival time of the Moho conversion into depth using the assumption that the average velocity above the Moho is 6.2 km s^{-1} and the v_P/v_S ratio is 1.73. The Moho depth was deduced between 12 and 13 km beneath the seismic refraction profiles (Charvis *et al.* 1999; Gallart *et al.* 1999) and underlain by an underplated magmatic

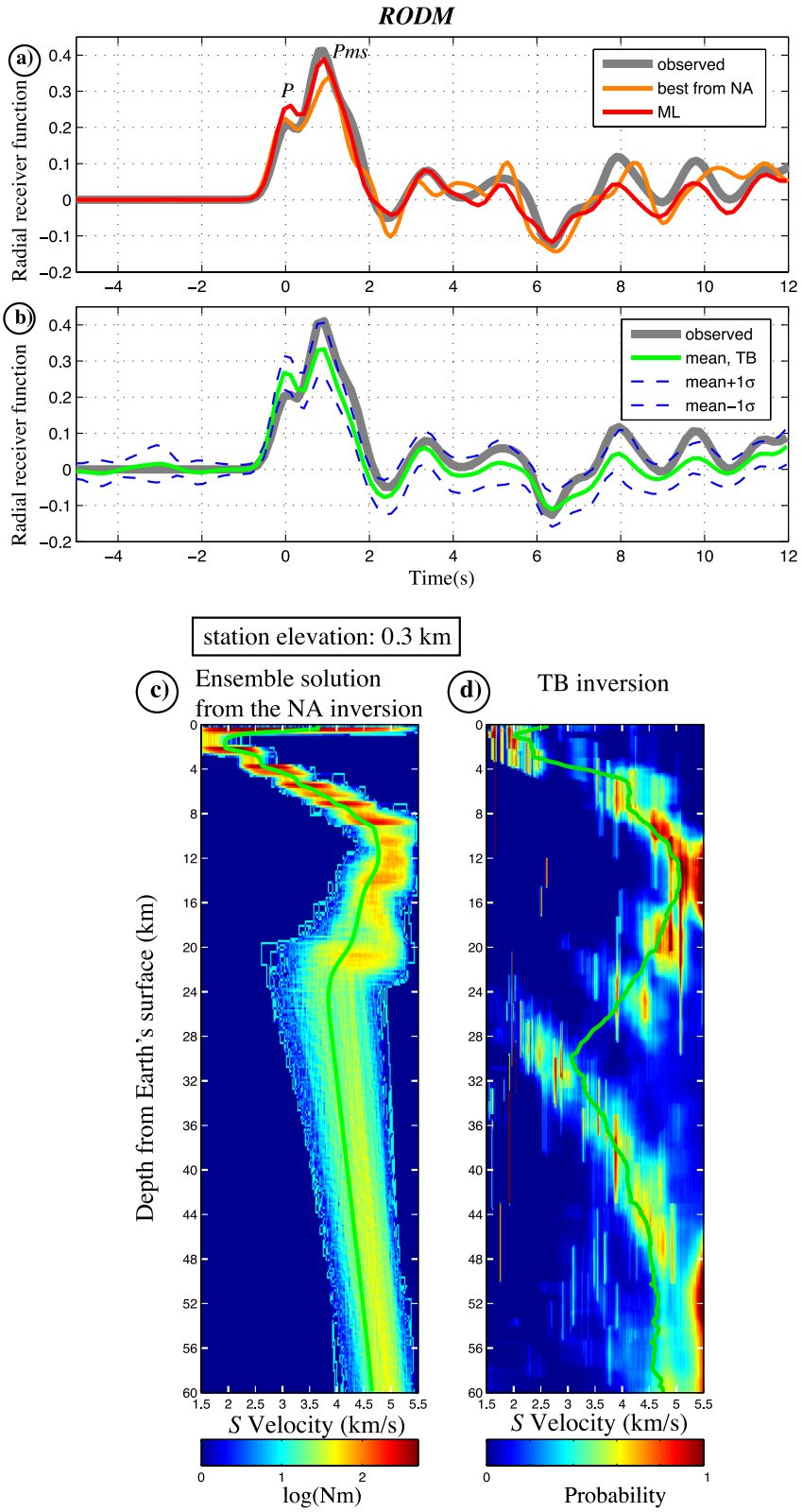

Figure 7. Results of RF inversions for station RODM. Description as in Fig. 3.

body of maximum 3 km (Fig. 2a). The Moho depth we determined in the present study (12 km) is therefore in agreement with previous results.

The fact that the first RF phase is characterized by a smaller peak than the *Pms* phase suggests a low velocity zone just below the surface. Leahy & Park (2005) also found a first peak smaller than the *Pms* phase at XMAS station (Kiribati) and a similar observation was realized at POHA station (on Big Island) for epicentral distance between 55° and 80° (Leahy *et al.* 2010). RF and SWD modelling suggests a sharp decrease of the

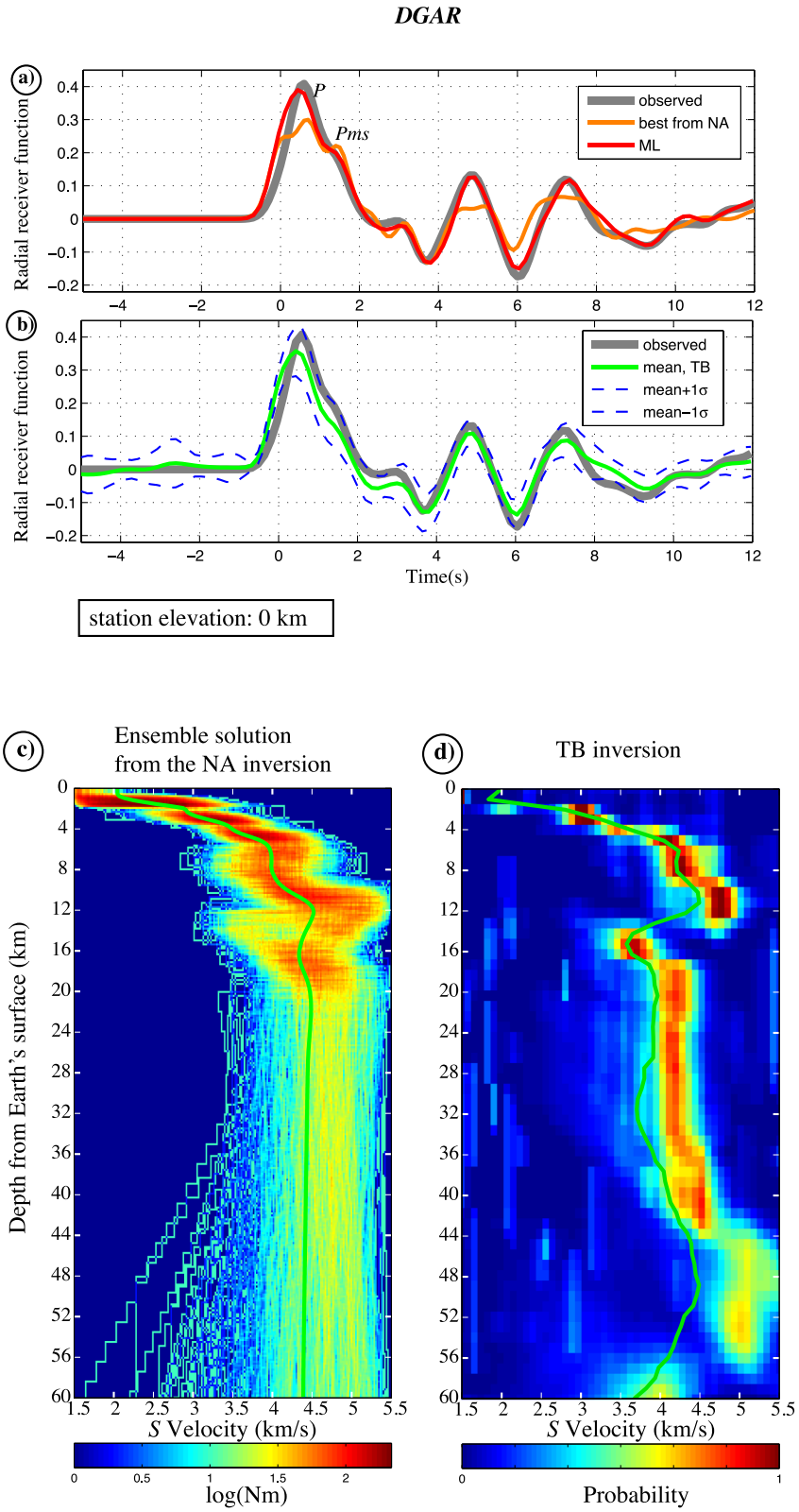

Figure 8. Results of RF inversions for station DGAR. Description as in Fig. 3.

velocity between 0 and 0.5 km bsl. Interestingly, Nercessian *et al.* (1996) observed that this range of depths corresponds to a decrease of local seismicity beneath the Piton de la Fournaise volcano. They also described a LVZ just beneath the sea level from 3-D velocity modelling of arrival times of seismic waves from local earthquakes and this LVZ was interpreted as a possible magma reservoir. The depth of the LVZ suggested beneath RER is also compatible with the range of depths 0–1 km above sea level of a LVZ imaged in a recent body-wave tomographic model (Prôno *et al.* 2009).

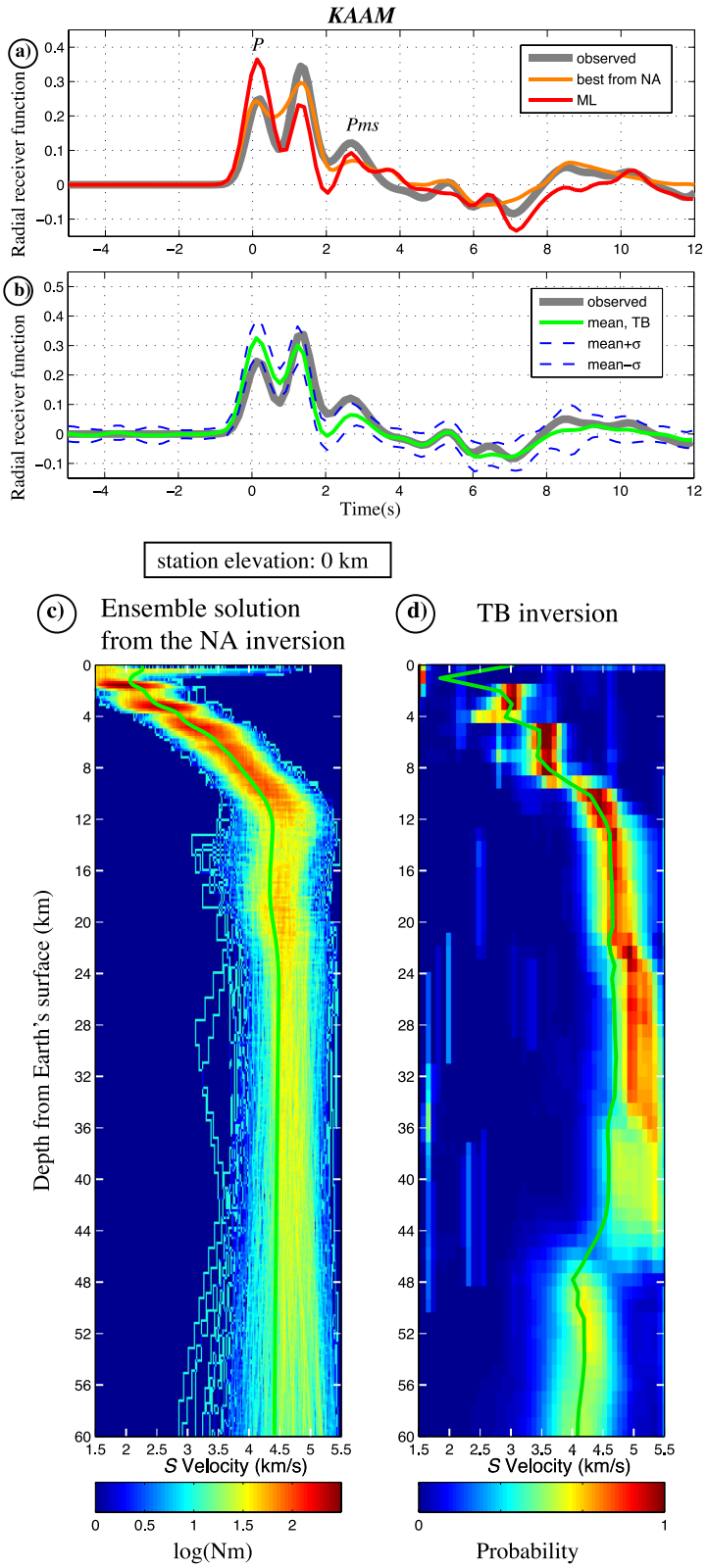

Figure 9. Results of RF inversions for station KAAM. Description as in Fig. 3.

Our estimate of the depth to the top of the oceanic crust (4 km bsl) is coherent with the regional bathymetry around La Réunion (Fig. 2d): around 4.2 km. The crustal thickness (*ca*. 6 km) is similar to normal oceanic crust thickness (6–7 km) in the CRUST 5.1 model (Mooney *et al.* 1998) and similar to the range of thicknesses (5–6 km) determined for the oceanic crust beneath La Réunion Island from seismic refraction profiles (Charvis *et al.* 1999).

The top of the LVZ observed in the upper mantle at about 33 km depth is close to a discontinuity imaged at around 30 km depth by seismic refraction with a minimum velocity contrast of 0.2 km s^{-1}

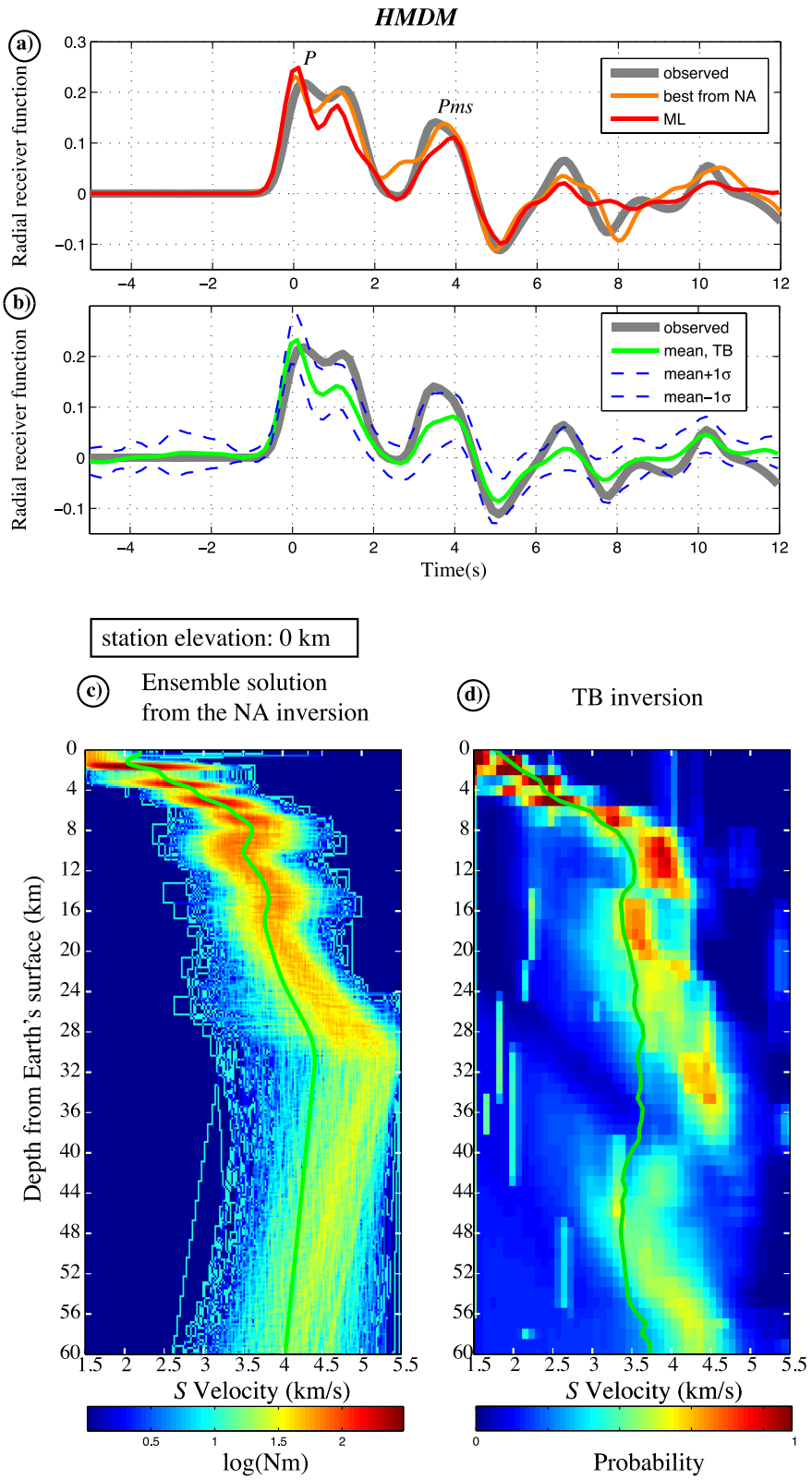

Figure 10. Results of RF inversions for station HMDM. Description as in Fig. 3.

(Gallart *et al.* 1999). The interface observed at 70 km depth is similar to a previous value determined from *P*-to-*s* converted phases (Rychert & Shearer 2009) and could represent the LAB.

Mauritius. Shor & Pollard (1963) proposed (from two-reversed seismic refraction profiles) the presence of an oceanic crust beneath Saya de Malha Bank. The presence of continental crust beneath Mauritius and part of the Southern Mascarene Plateau was proposed by Torsvik *et al.* (2013) from analysis of zircon xenocrysts found in Mauritius beach sand. The thick crust deduced from our analysis—17 km excluding the volcanic edifice thickness

Table 1. Station location and results of the RFs modelling with the NA and TB inversions at the permanent seismic stations. N_{cc} is the number of radial RFs with a cross-correlation coefficient ≥0.70 at the seismic station. *N* is the number of RFs used for the stacking at each station and *H* is the depth to mantle relative to sea level. Typical uncertainty of *H* is 2 km. *TC* is depth to top of crust relative to sea level. *Nature* represents the character of the Moho from the shear wave velocity model obtained with the NA and TB inversions at each station: thin ≤2 km, *inter* for intermediate 2–10 km and broad >10 km (modified from classification of Shibutani *et al.* 1996). *CT* is the crustal thickness without the underplated layer. *UP* is an estimation of the thickness of the underplated layer.

Station	Lat. (°)	Lon. (°)	Elevation (km)	N_{cc}	*N*	*TC* (km)	*H* (km)	*Nature*	*CT* (km)	*UP* (km)
RER	−21.1712	55.7399	0.8	29	14	4	12	Thin	6	2
MRIV	−20.2980	57.4970	0.4	12	5	4	21	Inter	10	7
RODM	−19.6962	63.4413	0.3	7	3	4	10	Thin	6	0
DGAR	−7.4121	72.4525	0.0	44	9	4	17	Inter	8	5
KAAM	0.4926	72.9949	0.0	11	4	5	23	Broad	7	11
HMDM	6.7731	73.1822	0.0	17	3	8	28	Broad	6	14

(Table 1)—and the apparent intermediate seismic velocity between 16 and 21 km bsl favour the presence of an oceanic crust with an underplated layer. However, we cannot reject from the analysis of a single station a possibility that small-scale continental crustal relics are embedded within the oceanic crust that could provide a source of the Precambrian zircons found at the surface on Mauritius (Torsvik *et al.* 2013). The velocity contrast ($v_P^{\text{lower layer}}/v_S^{\text{upper layer}}$) between an oceanic crust layer and an underplated magmatic layer is theoretically expected to be higher than between an underplated magmatic layer and the upper mantle. Therefore, stronger amplitude on RF is expected for the converted phase at the top of an underplated magmatic layer, which could explain why, for instance, the *H*–κ stacking results at MRIV suggest a Moho depth at ∼15 km (Appendix D).

Chagos. Seismic refraction investigations (Francis & Shor 1966) suggest a Moho depth of at least 20 km at around 230 km north–northeast of DGAR station (Diego Garcia atoll). Henstock & Thompson (2004) determined north of Diego Garcia an average crustal thickness of 27 km beneath the Chagos Bank (at ∼6°S) from model of bathymetry and gravity data. In this study, RF inversions suggest a shallower Moho depth at DGAR station (∼17 km).

Maldives. Torsvik *et al.* (2013) suggested (from gravity anomaly inversion) a crustal thickness ≥25–30 km beneath the Laccadives, Maldives and Chagos. A Moho depth of at least 20 km was suggested around 240 km south of KAAM station by a seismic refraction experiment (Francis & Shor 1966). The depths obtained in this study are therefore compatible with their results.

6.2 Estimates of lithospheric thickness beneath La Réunion, Mauritius and Rodrigues

RODM station is installed on a relatively young lithosphere (*ca.* 13 Ma). Using the simple assumption that the oceanic lithosphere thickness is controlled by the plate cooling and therefore related to the plate age (e.g. Fowler 1990), a lithospheric thickness of ∼33 km is theoretically expected beneath Rodrigues Island. Our RF measurements at RODM indicate a clear low velocity layer starting at 25 km depth, which is in agreement with this theoretical value provided by a simple cooling law (e.g. Fowler 1990).

RER and MRIV stations are located on a relatively old lithosphere (*ca.* 67 and 72 Ma, respectively). The complexity of magnetic anomalies pattern around La Réunion and Mauritius (Dyment 1991, 1993; Bissessur 2011) suggests heterogeneous lithosphere. Assuming that the oceanic lithosphere thickening is controlled by the plate cooling and thus related to the plate age (e.g. Fowler 1990), the lithospheric thickness is estimated at ∼74 km beneath RER and ∼77 km beneath MRIV. Our joint inversion results clearly show that this assumption may be valid for RER. We indeed observe a discontinuity at ∼70 km depth beneath La Réunion that may correspond to the base of the mantle lid, and thus to a normal lithospheric thickness. This observation is deduced from the inversion of both RF and SWD data, and has a larger scale meaning than from the inversion of RF alone. Such lithosphere thickness is not incompatible with features such as the low velocity layer visible at ∼33 km discussed below, that may suggest partial melt or hot material, the lateral extent of which being at least of the order of 10 km but poorly constrained at larger scale. One can indeed imagine that an almost normal LAB may exist beneath La Réunion together with the presence of more superficial small-scale body of partial melting and of short scale isotherms upwellings. Beneath Mauritius, our results indicate that a LVZ upper interface is located at about 50 km depth. If this interface represents the same layer visible at about 70 km depth beneath La Réunion, the presence of a shallower LAB beneath MRIV suggests a large-scale lithospheric thinning, which could be an effect of the plume–lithosphere interaction.

Such interpretation is compatible with numerical modelling of thermomechanical erosion of the lithosphere by heat conduction due to an interaction with the mantle plume. Thoraval *et al.* (2006) have shown that such erosion could reach 30 km. Recent numerical simulations from Agrusta *et al.* (2013) also show up to 20 km of plate thinning but also that the motion of the lithosphere far from the hotspot results in rethickening of the lithosphere. Thermomechanical erosion of the base of the lithosphere may therefore explain the LVZ observed at 50 km beneath MRIV, which is observed at 70 km beneath La Réunion, as schematized in Fig. 11. The lithosphere thinning from La Réunion to Mauritius, if any, is similar to that described for Hawaii. Li *et al.* (2004) from *S* receiver function analysis indeed proposed a progressive lithospheric thinning from 108 km beneath the Big Island of Hawaii to *ca.* 54 km towards Kauai, located about 500 km away from Big Island. Bonneville *et al.* (1995, 1997) performed heat flow measurements along two seismic profiles across the Mascarene Ridge (Fig. 2a). Their results suggest rejuvenation of the lithosphere below the Mascarene ridge and normal lithosphere beneath La Réunion. This confirms previous analysis of the geoid/bathymetry by Bonneville *et al.* (1988) showing a much stronger lithosphere around La Réunion Island than around Mauritius Island.

6.3 Magmatic underplating beneath the hotspot track

Underplating magmatic body is referred here to preferential ponding of melt in the shallowest mantle below an initial crust (e.g.

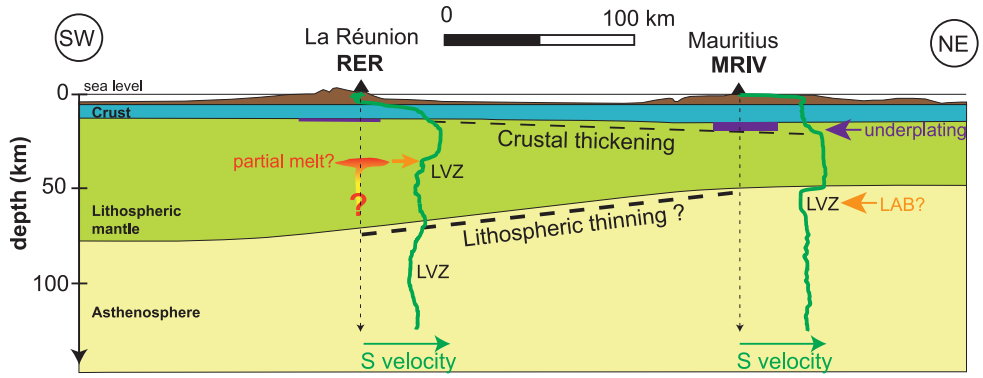

Figure 11. Cartoon summarizing the joint inversion findings obtained in this study in the area covering La Réunion and Mauritius islands. Green curves show the 1-D shear wave velocity profile obtained from joint inversion at RER and at MRIV seismic stations. The LVZ evidenced at around 33 km beneath RER may be due to the presence of partial melt as suggested by geochemical studies and/or high temperature. A crustal thickening is suggested from La Réunion to Mauritius, whereas the lithospheric thickness seems smaller beneath Mauritius than beneath La Réunion. LAB represents the possible depth of the lithosphere asthenosphere boundary.

Gallart *et al.* 1999; Leahy *et al.* 2010) due to a density barrier. Ultramafic magmatic underplating was evidenced by seismic refraction images at the base of the crust beneath active oceanic hotspots such as Hawaii, Marquesas and La Réunion (e.g. Watts *et al.* 1985; Caress *et al.* 1995; Charvis *et al.* 1999). A magmatic underplated body is expected to produce a gradational crust - mantle transition with seismic velocities intermediate between standard lower crust and the uppermost mantle. *P*-wave velocities between 7.5 and 8.0 km s^{-1} characterize this magmatic body (e.g. Watts *et al.* 1985; Caress *et al.* 1995; Charvis *et al.* 1999). Leahy *et al.* (2010) show from RF analysis the possible presence of a 5-km-thick underplated layer beneath KIP station (on Oahu) and 9-km beneath POHA station (on Big Island). It is interpreted as rocks with greater proportions of olivine and pyroxene than rocks in the 'normal' oceanic lower-crust (Richards *et al.* 2013). Richards *et al.* (2013) proposed that this underplated magmatic body is due to melting of hot rising plume material beneath mature oceanic lithosphere at around 2–3 GPa (60–90 km depth). Ultramafic melts then pond and undergo olivine and clinopyroxene fractionation at the Moho due to their relatively high density.

Interestingly in this study, no underplated magmatic body is found from RF inversions at RODM (Rodrigues), which is the only station that is not located on the hotspot track. On the other hand, the presence of underplated material is clearly argued beneath RER (La Réunion), MRIV (Mauritius), DGAR (Diego Garcia), KAAM and HMDM (two atolls of Maldives) that are all located on the hotspot track. The ~2-km-thick body determined in this study at RER is compatible with the thickness estimated from seismic refraction profiles (Charvis *et al.* 1999; Gallart *et al.* 1999). Magmatic underplating appears however to be rather heterogeneous beneath La Réunion since no apparent crustal underplating was postulated beneath the north-eastern flank of the island and between the La Réunion and Mauritius islands (Charvis *et al.* 1999). The underplated body was indeed described as elongated perpendicularly to the presumed hotspot track (Fig. 2a) and may not be controlled by the present-day plate motion.

Magmatic underplating was described at other places in the western Indian Ocean near or on the trace of the Réunion hotspot suggesting a link with the Réunion plume. At the base of the crust in Saurashtra and other parts of western India a thick (8–10 km) underplated layer is suggested from deep seismic sounding studies (Kaila *et al.* 1990; Rao & Tewari 2005) and may be due to the passage of India over the Réunion plume in the Late Cretaceous. Beneath the Laxmi Ridge, Minshull *et al.* (2008) also argued for the presence of an underplated magmatic body between 13 and 23 km from wide-angle seismic data. They propose that this layer was formed by lateral melt migration from the Réunion plume at the time the Laxmi Ridge was close to India. At this time, Seychelles was possibly attached to the Laxmi Ridge (e.g. Hammond *et al.* 2013; Torsvik *et al.* 2013). The thinning of an underplated layer southwards from ~10 km to 1 km was suggested by Hammond *et al.* 2013 from RF analysis obtained at Praslin and Mahé (two islands of Seychelles archipelago). This underplating was also attributed to the Réunion plume at the time before the rifting of the Seychelles from the Indian continent. The Laccadive Ridge is located north of the Maldives and it was proposed to be on the trace of the Réunion plume (e.g. Morgan 1972). Interestingly, Gupta *et al.* (2010) estimated the presence of an underplated layer of 8 km thick and a Moho depth of 24 km from RF analysis on Minicoy Island (on the Laccadive Ridge).

All the above observations show the ubiquitous presence of underplated material in relation with the hotspot activity. The large spatial variation in the thickness distribution may be interpreted by several ways:

(1) The arrival of blobs or solitary waves of plume material at the base of the plate as suggested by geochemical studies of the Piton de la Fournaise and the Piton des Neiges volcanoes (Albarède *et al.* 1997; Bosch *et al.* 2008), suggesting that they were formed by a single large heterogeneous plume with two small-scale blobs characterized by different composition;

(2) The large-scale spreading of mantle plume material at scale of hundreds of kilometres that may generate several local and independent instabilities within the asthenosphere, each inducing local partial melt and local volcanic activity. Such sublithospheric spreading of the Réunion mantle plume was suggested by Barruol & Fontaine (2013) to explain the *SKS* observations at seismic stations located on La Réunion and Mauritius Islands. They proposed a plume upwelling located north of La Réunion and spreading within the asthenosphere that could best explain their *SKS* splitting measurements. Such interpretation explains well our present observations of thinner underplated material beneath La Réunion (located upstream) than beneath Mauritius (located downstream of the plume conduit).

6.4 Hotspot-related LVZ beneath La Réunion

From our joint inversion results, a LVZ is clearly evidenced beneath La Réunion at about 33 km depth. Interestingly, the seismic refraction measurements performed by Gallart *et al.* (1999) also suggested a seismic discontinuity imaged at 26–32 km depth over a profile of ∼78 km long. Such a low velocity at lithospheric depth may have various origins. To interpret low *S*-wave velocities in the upper mantle beneath the Seychelles, Hammond *et al.* (2012) proposed the effect of residual sulphide melt left from the Deccan plume. An increase of the temperature in the upper mantle could also decrease the shear wave velocity, as suggested by laboratory measurements of the shear modulus (e.g. Tan *et al.* 1997; Jackson *et al.* 2002) and that could contribute to the presence of a LVZ. From the strength of the signal we observed beneath La Réunion, we propose that the detected LVZ likely results from both high temperature and partial melt or magma locally stored at those depths. This interpretation is compatible with several geochemical studies. The analysis of the Piton de la Fournaise lavas suggests melt differentiation of the magma from more than 15 km depth (e.g. Albarède & Tamagnan 1988; Bureau *et al.* 1998). Albarède *et al.* (1997) proposed the existence of a deep olivine plus clinopyroxene crystalline mush beneath the Piton de la Fournaise volcano. Recently, Boivin & Bachèlery (2009) included this deep mush in their conceptual model of the magma storage system of the Piton de la Fournaise in order to explain the origin of a type of magma erupted during March 1998 eruption.

The lateral extent of such LVZ is however poorly constrained by our RF measurements: the radius of the first Fresnel zone, i.e., the distance from the seismic station sampled by the *Pms* phase, is about 10 km for a seismic discontinuity at 30 km depth (if we assume a dominant frequency of 0.4 Hz and a crustal *S*-wave velocity of 3.46 km s^{-1}). The sampling of this LVZ by the single RER seismic station does not provide any clues to discriminate between a zone of partial melt embedded within the lithosphere and a zone of partial melt storage bottoming an extremely thinned lithosphere. As explained above, the presence of a low velocity zone beneath 70 km depth favours a normal lithospheric thickness beneath La Réunion, as illustrated on the cartoon in Fig. 11 summarizing the main features observed beneath La Réunion and Mauritius.

The interpretation of 'punctual' RF measurements beneath the island requires more extensive analyses to decipher the lateral extent and continuity of the observed interfaces that represent key questions concerning the plume-lithosphere interaction and the shape of the magma storage system.

7 CONCLUSION

Receiver function modelling of broad-band seismic waveforms recorded at permanent seismic stations located in the Western Indian Ocean has been applied to constrain the crustal and upper mantle structure beneath La Réunion hotspot track, and the interaction between the Réunion plume and the oceanic lithosphere. Joint inversion of receiver function and surface wave dispersion data was also performed at RER and MRIV. Receiver function measurements evidence a shallow Moho (12 km deep) beneath the active hotspot area in La Réunion and clearly deeper Moho (between 17 and 28 km deep) beneath the other seismic stations installed on the fossil part of the presumed hotspot track. Underplated material is detected beneath all sites except Rodrigues, which is not on the plume track. The thinnest underplated layer is likely beneath the Piton de la Fournaise volcano. Such ubiquitous presence of underplated material suggests that a large part of the plume magmatic production is likely trapped at the base of the crust and that just a small fraction reaches the surface. A striking feature we observed in the mantle beneath La Réunion is a low velocity zone detected at shallow depth (∼33 km), but absent beneath the other stations located on the older part of the hotspot track. We propose that this LVZ likely represents partial melt storage area beneath the active volcano. Joint inversions of RF and SWD data finally suggest that the lithosphere is likely ∼70 km thick beneath La Réunion (at least at large-scale) but appears to be thinner beneath Mauritius, which is compatible with possible lithospheric erosion induced by a mantle upwelling.

A denser sampling of the lithosphere such as the one performed by the recently deployed RHUM-RUM temporary seismic network (Barruol & Sigloch 2013) should help future studies to better constrain the Réunion plume-lithosphere interaction and particularly the lateral and vertical extents of the lithosphere thinning and of the LVZ and their relations with the possible plume location at depth.

ACKNOWLEDGEMENTS

We thank M.S. Sambridge for his NA inversion program and L. Michon, J. Dyment, J. Morgan, V. Famin and N.M. Vitry for fruitful discussions. The constructive comments of three anonymous reviewers have been appreciated. Thanks to the GEOSCOPE and GEOFON network for the maintenance and availability of the high quality seismic data. The facilities of IRIS Data Services, and specifically the IRIS Data Management Center, were used for access to waveforms, related metadata, and/or derived products used in this study. IRIS Data Services are funded through the Seismological Facilities for the Advancement of Geoscience and EarthScope (SAGE) Proposal of the National Science Foundation under Cooperative Agreement EAR-1261681. We are grateful to the TITAN (University of La Réunion) and TerraWulf (The Australian National University) computational clusters. Thomas Bodin acknowledges support from the Miller Institute for Basic Research at the University of California, Berkeley. This work was supported by the Institut de Physique du Globe, Paris. This is IPGP contribution 3648.

REFERENCES

Agrusta, R., Arcay, D., Tommasi, A., Davaille, A., Ribe, N. & Gerya, T., 2013. Small-scale convection in a plume-fed low-viscosity layer beneath a moving plate, *Geophys. J. Int.,* **194,** 591–610.

Albarède, F. & Tamagnan, V., 1988. Modelling the recent geochemical evolution of the Piton de la Fournaise volcano, Réunion island, 1931–1986, *J. Petrol.,* **29,** 997–1030.

Albarède, F., Luais, B., Fitton, G., Semet, M., Kaminski, E., Upton, B.G.J., Bachèlery, P. & Cheminée, J.-L., 1997. The Geochemical Regimes of Piton de la Fournaise Volcano (Réunion) during the last 530 000 years, *J. Petrol.,* **38,** 171–201.

Bannister, S., Yu, J., Leitner, B. & Kennett, B.L.N., 2003. Variations in crustal structure across the transition from West to East Antarctica, Southern Victoria Land, *Geophys. J. Int.,* **155,** 870–884.

Barruol, G. & Fontaine, F.R., 2013. Mantle flow beneath La Réunion hotspot track from *SKS* splitting, *Earth planet. Sci. Lett.,* **362,** 108–121.

Barruol, G. & Sigloch, K., 2013. Investigating La Réunion hot spot from crust to core, *EOS, Trans. Am. geophys. Un.,* **94**(23), 205–207.

Bayes, T., 1763. An essay towards solving a problem in the doctrine of chances, *Phil. Trans. R. Soc. Lond.,* **53,** 370–418. (Reprinted, with biographical note by Barnard, G.A., 1958, Biometrika 45, 293–315).

Bissessur, P.D., 2011. Structure, age and evolution of the Mascarene basin, Western Indian Ocean, *PhD thesis,* IPGP, Paris, France, 183 pp.

Bodin, T., Sambridge, M., Tkalčić, H., Arroucau, P., Gallagher, K. & Rawlinson, N., 2012a. Transdimensional inversion of receiver functions and surface wave dispersion, *J. geophys. Res.,* **117,** B02301, doi:10.1029/2011JB008560.

Bodin, T., Sambridge, M., Rawlinson, N. & Arroucau, P., 2012b. Transdimensional tomography with unknown data noise, *Geophys. J. Int.,* **189,** 1536–1556.

Boivin, P. & Bachèlery, P., 2009. Petrology of 1977 to 1998 eruptions of Piton de la Fournaise, La Réunion Island, *J. Volc. Geotherm. Res.,* **184,** 109–125.

Bonneville, A., Barriot, J.P. & Bayer, R., 1988. Evidence from geoid data of a hotspot origin for the Southern Mascarene Plateau and Mascarene Islands (Indian Ocean), *J. geophys. Res.,* **93,** 4199–4212.

Bonneville, A., Von Herzen, R.P. & Lucazeau, F., 1997. Heat flow over Reunion hot spot track: Additional evidence for thermal rejuvenation of oceanic lithosphere, *J. geophys. Res.,* **102,** 22 731–22 747.

Bonneville, A., Von Herzen, R.P., Lucazeau, F. & Provost, A. Scientific Party of MD72, 1995. Une lithosphère amincie sous le point chaud de la Réunion? Contraintes apportées par de nouvelles mesures de flux de chaleur sur la ride des Mascareignes, *C. R. Acad. Sc. Paris,* **321**(II), 909–915.

Bosch, D., Blichert-Toft, J., Moynier, F., Nelson, B.K., Telouk, P., Gillot, P.-Y. & Albarède, F., 2008. Pb, Hf and Nd isotope compositions of the two Réunion volcanoes (Indian Ocean): a tale of two small-scale mantle "blobs"?, *Earth planet. Sci. Lett.,* **265,** 748–768.

Brenguier, F., Shapiro, N.M., Campillo, M., Nercessian, A. & Ferrazzini, V., 2007. 3-D surface wave tomography of the Piton de la Fournaise volcano using seismic noise correlations, *Geophys. Res. Lett.,* **34,** doi:10.1029/2006GL028586.

Burdick, L. & Langston, C., 1977. Modeling crustal structure through the use of converted phases in teleseismic body-wave forms, *Bull. seism. Soc. Am.,* **67,** 677–691.

Bureau, H., Métrich, N., Pineau, F. & Semet, M.P., 1998. Magma–conduit interaction at Piton de la Fournaise volcano (Réunion Island): a melt and fluid inclusion study, *J. Volc. Geotherm. Res.,* **84,** 39–60.

Burke, K., 1996. The African plate, *South Afr. J. Geol.,* **99,** 339–408.

Caress, D.W., McNutt, M.K., Detrick, R.S. & Mutter, J.C., 1995. Seismic imaging of hotspot-related crustal underplating beneath the Marquesas Islands, *Nature,* **373,** 600–603.

Charvis, P. *et al.*, 1999. Spatial distribution of hotspot material added to the lithosphere under La Réunion, from wide-angle seismic data, *J. geophys. Res.,* **104,** 2875–2893.

Courtillot, V., Besse, J., Vandamme, D., Montigny, R., Jaeger, J.-J. & Cappetta, H., 1986. Deccan flood basalts at the Cretaceous/Tertiary boundary, *Earth planet. Sci. Lett.,* **80,** 361–374.

Courtillot, V., Davaille, A., Besse, J. & Stock, J., 2003. Three distinct types of hotspots in the Earth's mantle, *Earth planet. Sci. Lett.,* **205,** 295–308.

Deniel, C., Kieffer, G. & Lecointre, J., 1992. New ^{230}Th-^{238}U and ^{14}C age determinations from Piton des Neiges volcano, Reunion—a revised chronology for the differentiated series, *J. Volc. Geotherm. Res.,* **51,** 253–267.

Dettmer, J., Dosso, S.E. & Holland, C., 2010. Trans-dimensional geoacoustic inversion, *J. acoust. Soc. Am.,* **128,** 3393–4005.

Devey, C. & Stephens, W.E., 1991. Tholeiitic dykes in the Seychelles and the original spatial extent of the Deccan, *J. Geol. Soc. Lond.,* **148,** 979–983.

Du, Z.J. & Foulger, G.R., 1999. The crustal structure beneath the northwest fjords, Iceland, from receiver functions and surface waves, *Geophys. J. Int.,* **139,** 419–432.

Duncan, R.A., 1981. Hotspots in the Southern Oceans—an absolute frame of reference for motion of the Gondwana continents, *Tectonophysics,* **74,** 29–42.

Duncan, R.A., 1990. The volcanic record of the Reunion hotspot, in *Proceedings of the Ocean Drilling Program, Scientific Results,* Vol. 115, pp. 3–10, eds Duncan, R.A., Backman, J. & Peterson, L.C., Ocean Drilling Program, College Station, TX.

Duncan, R.A. & Hargraves, R.B., 1990. ^{40}Ar/^{39}Ar Geochronology of basement rocks from the Mascarene plateau, the Chagos bank and the Maldives ridge, in *Proceedings of the Ocean Drilling Program, Scientific Results,* Vol. 115, pp. 43–51, eds Duncan, R.A., Backman, J. & Peterson, L.C., Ocean Drilling Program, College Station, TX.

Dyment, J., 1991. Structure et évolution de la lithosphère océanique dans l'Océan Indien: Apport des anomalies magnétiques, *PhD thesis,* Univ. de L. Pasteur, Strasbourg, France, 374 pp.

Dyment, J., 1993. Evolution of the Indian Ocean Triple Junction Between 65 and 49 Ma (Anomalies 28 to 21), *J. geophys. Res.,* **98,** 13 863–13 877.

Dyment, J., Lin, J. & Baker, E.T., 2007. Ridge-hot spot interactions: What mid-ocean ridges tell us about deep Earth processes, *Oceanography,* **20,** 102–115.

Fontaine, F.R., Tkalčić, H. & Kennett, B.L.N., 2013a. Imaging crustal structure variation across southeastern Australia, *Tectonophysics,* **582,** 112–125.

Fontaine, F.R., Tkalčić, H. & Kennett, B.L.N., 2013b. Crustal complexity in the Lachlan Orogen revealed from teleseismic receiver functions, *Aust. J. Earth Sci.,* **60**(3), 413–430.

Fowler, C.M.R., 1990. *The Solid Earth: An Introduction to Global Geophysics,* Cambridge Univ. Press, 472 pp.

Francis, T.J.G. & Shor, G.G. Jr, 1966. Seismic refraction measurements in the northwest Indian Ocean, *J. geophys. Res.,* **71,** 427–449.

Füri, E., Hilton, D.R., Murton, B.J., Hémond, C., Dyment, J. & Day, J.M.D., 2011. Helium isotope variations between Réunion Island and the Central Indian Ridge (17°–21°S): new evidence for ridge-hot spot interaction, *J. geophys. Res.,* **116,** B02207, doi:10.1029/2010JB007609.

Gallagher, K., Bodin, T., Sambridge, M., Weiss, D., Kylander, M. & Large, D., 2011. Inference of abrupt changes in noisy geochemical records using transdimensional changepoint models, *Earth planet. Sci. Lett.,* **311,** 182–194.

Gallart, J., Driad, L., Charvis, P., Sapin, M., Hirn, H., Diaz, J., De Voogd, B. & Sachpazi, M., 1999. Perturbation to the lithosphere along the hotspot track of La Réunion from an offshore-onshore seismic transect, *J. geophys. Res.,* **104,** 2895–2908.

Gillot, P.-Y., Lefèvre, J.-C. & Nativel, P.-E., 1994. Model for the structural evolution of the volcanoes of Réunion Island, *Earth planet. Sci. Lett.,* **122,** 291–302.

Gillot, P.-Y. & Nativel, P., 1989. Eruptive history of the Piton de la Fournaise volcano, Réunion Island, Indian Ocean, *J. Volc. Geotherm. Res.,* **36,** 53–65.

Green, P.J., 1995. Reversible jump Markov chain Monte Carlo computation and Bayesian model determination, *Biometrika,* **82,** 711–732.

Green, P.J., 2003. Trans-dimensional Markov chain Monte Carlo, in *Highly Structured Stochastic Systems,* pp. 179–198, eds Green, P.J., Hjort, N.L. & Richardson, S., Oxford Statistical Science Series, Oxford Univ. Press.

Gripp, A.E. & Gordon, R.G., 1990. Current plate velocities relative to the hotspots incorporating the NUVEL-1 global plate motion model, *Geophys. Res. Lett.,* **17,** 1109–1112.

Gupta, S., Mishra, S. & Rai, S.S., 2010. Magmatic underplating of crust beneath the Laccadive Island, NW Indian Ocean, *Geophys. J. Int.,* **183,** 536–542.

Hammond, J.O.S., Collier, J.S., Kendall, J.M., Helffrich, G. & Rümpker, G., 2012. Plume scar in the mantle lithosphere beneath the Seychelles revealed by seismic imaging, *Earth planet. Sci. Lett.,* **355–356,** 20–31.

Hammond, J.O.S., Kendall, J.M., Collier, J.S. & Rümpker, G., 2013. The extent of continental crust beneath the Seychelles, *Earth planet. Sci. Lett.,* **381,** 166–176.

Haskell, N.A., 1953. The dispersion of surface waves in multilayered media, *Bull. seism. Soc. Am.,* **43,** 17–34.

Haskell, N.A., 1962. Crustal reflection of plane *P* and *SV* waves, *J. geophys. Res.,* **67,** 4751–4767.

Henstock, T.J. & Thompson, P.J., 2004. Self-consistent modeling of crustal thickness at Chagos–Laccadive ridge from bathymetry and gravity data, *Earth planet. Sci. Lett.,* **224,** 325–336.

Hopcroft, P.O., Gallagher, K. & Pain, C.C., 2009. A Bayesian partition modelling approach to resolve spatial variability in climate records from borehole temperature inversion, *Geophys. J. Int.,* **178,** 651–666.

Iaffaldano, G., Bodin, T. & Sambridge, M., 2012. Reconstructing plate-motion changes in the presence of finite-rotations noise, *Nat. Commun.,* **3,** 1048, doi:10.1038/ncomms2051.

Jackson, I., Fitz Gerald, J.D., Faul, U.H. & Tan, B.H., 2002. Grain-size-sensitive seismic wave attenuation in polycrystalline olivine, *J. geophys. Res.,* **107**(B12), 2360, doi:10.1029/2001JB001225.

Juliá, J., Ammon, C., Herrmann, R. & Correig, A., 2000. Joint inversion of receiver function and surface wave dispersion observations, *Geophys. J. Int.,* **143,** 99–112.

Kaila, K.L., Tewari, H.C., Krishna, V.G., Dixit, M.M., Sarkar, D. & Reddy, M.S., 1990. Deep seismic sounding studies in the north Cambay and Sanchor basins, India, *Geophys. J. Int.,* **103,** 621–637.

Kennett, B.L.N., 1983. *Approximations to the Response of the Stratification, in Seismic Wave Propagation in Stratified Media,* Chapter 9, Cambridge Univ. Press, New York, pp. 177–208.

Lamarque, G., Barruol, G., Fontaine, F.R., Bascou, J. & Menot, R.P., 2015. Crustal and mantle structure beneath the Terre Adelie Craton, East Antarctica: insights from receiver function and seismic anisotropy measurements, *Geophys. J. Int.,* **200,** 809–823.

Langston, C.A., 1977. Corvallis, Oregon, crustal and upper mantle receiver structure from teleseismic *P* and *S* waves, *Bull. seism. Soc. Am.,* **67,** 713–724.

Langston, C.A., 1979. Structure under Mount Rainier, Washington, inferred from teleseismic body waves, *J. geophys. Res.,* **84,** 4749–4762.

Leahy, G., Collins, J.A., Wolfe, C.J., Laske, G. & Solomon, S.C., 2010. Underplating of the Hawaiian Swell: evidence from teleseismic receiver functions, *Geophys. J. Int.,* **183,** 313–329.

Leahy, G.M. & Park, J., 2005. Hunting for oceanic island Moho, *Geophys. J. Int.,* **160,** 1020–1026.

Lénat, J.-F., Gibert-Malengreau, B. & Galdéano, A., 2001. A new model for the evolution of the volcanic island of Réunion (Indian Ocean), *J. geophys. Res.,* **106,** 8645–8663.

Li, X., Kind, R. & Yuan, X., 2003. Seismic study of upper mantle and transition zone beneath hotspots, *Phys. Earth planet. Inter.,* **136,** 79–92.

Li, X., Kind, R., Yuan, X., Wölbern, I. & Hanka, W., 2004. Rejuvenation of the lithosphere by the Hawaiian plume, *Nature,* **427,** 827–829.

Ligorria, J.P. & Ammon, C.J., 1999. Iterative deconvolution and receiver function estimation, *Bull. seism. Soc. Am.,* **89,** 1395–1400.

Ma, Z., Masters, G., Laske, G. & Pasyanos, M., 2014. A comprehensive dispersion model of surface wave phase and group velocity for the globe, *Geophys. J. Int.,* **199,** 113–135.

Malengreau, B., Lénat, J.-F. & Froger, J.-L., 1999. Structure of Réunion Island (Indian Ocean) inferred from the interpretation of gravity anomalies, *J. Volc. Geotherm. Res.,* **88,** 131–146.

Malinverno, A., 2002. Parsimonious Bayesian Markov chain Monte Carlo inversion in a nonlinear geophysical problem, *Geophys. J. Int.,* **151,** 675–688.

McDougall, I., 1971. The geochronology and evolution of the young volcanic island of Réunion, Indian Ocean, *Geochim. cosmochim. Acta,* **35,** 261–288.

McDougall, I., Upton, B.G.J. & Wadsworth, W.J., 1965. A geological reconnaissance of Rodriguez Island, Indian Ocean, *Nature,* **206,** 26–27.

Michon, L., Saint-Ange, F., Bachèlery, P., Villeneuve, N. & Staudacher, T., 2007. Role of the structural inheritance of the oceanic lithosphere in the magmato-tectonic evolution of Piton de la Fournaise volcano (La Réunion Island), *J. geophys. Res.,* **112,** doi:10.1029/2006JB004598.

Minshull, T.A., Lane, C.I., Collier, J.S. & Whitmarsh, R.B., 2008. The relationship between rifting and magmatism in the northeastern Arabian Sea, *Nat. Geosci.,* **1,** 463–467.

Montelli, R., Nolet, G., Dahlen, F.A., Masters, G., Engdahl, E.R. & Hung, S.-H., 2004. Finite-frequency tomography reveals a variety of plumes in the mantle, *Science,* **303,** 338–343.

Mooney, W.D., Laske, G. & Masters, T.G., 1998. CRUST 5.1: a global crustal model at $5^\circ \times 5^\circ$, *J. geophys. Res.,* **103,** 727–747.

Moore, J., White, W.M., Paul, D., Duncan, R.A., Abouchami, W. & Galer, S.J.G., 2011. Evolution of shield-building and rejuvenescent volcanism of Mauritius, *J. Volc. Geotherm. Res.,* **207,** 47–66.

Morgan, W.J., 1971. Convection plumes in the lower mantle, *Nature,* **230,** 42–43.

Morgan, W.J., 1972. Plate motions and deep mantle convection, *Geol. Soc. Am. Mem.,* **132,** 7–22.

Morgan, W.J., 1978. Rodriguez; Darwin, Amsterdam—a second type of hotspot island, *J. geophys. Res.,* **83,** 5355–5360.

Nercessian, A., Hirn, A., Lépine, J.C. & Sapin, M., 1996. Internal structure of Piton de la Fournaise volcano from seismic wave propagation and earthquake distribution, *J. Volc. Geotherm. Res.,* **70,** 123–143.

O'Neill, C., Müller, D. & Steinberger, B., 2005. On the uncertainties in hot spot reconstructions and the significance of moving hot spot reference frames, *Geochem. Geophys. Geosyst.,* **6,** 1–35.

Özalaybey, S., Savage, M.K., Sheehan, A.F., Louie, J.N. & Brune, J.N., 1997. Shear-wave velocity structure in the northern basin and range province from the combined analysis of receiver functions and surface waves, *Bull. seism. Soc. Am.,* **87,** 183–189.

Pasyanos, M.E., Masters, T.G., Laske, G. & Ma, Z., 2014. LITHO1.0: an updated crust and lithospheric model of the Earth, *J. geophys. Res.,* **119,** 2153–2173.

Peng, X. & Humphreys, E.D., 1997. Moho dip and crustal anisotropy in northwestern Nevada from teleseismic receiver functions, *Bull. seism. Soc. Am.,* **87,** 745–754.

Phinney, R., 1964. Structure of the Earth's crust from spectral behavior of long-period body waves, *J. geophys. Res.,* **69,** 2997–3017.

Piana Agostinetti, N. & Malinverno, A., 2010. Receiver function inversion by trans-dimensional Monte Carlo sampling, *Geophys. J. Int.,* **181,** 858–872.

Prôno, E., Battaglia, J., Monteiller, V., Got, J.-L. & Ferrazzini, V., 2009. P-wave velocity structure of Piton de la Fournaise volcano deduced from seismic data recorded between 1996 and 1999, *J. Volc. Geotherm. Res.,* **184,** 49–62.

Rançon, J.Ph., Lerebour, P. & Augé, T., 1989. The Grand Brûlé exploration drilling: new data on the deep framework of the Piton de la Fournaise volcano. Part 1: lithostratigraphic units and volcanostructural implications, *J. Volc. Geotherm. Res.,* **36,** 113–127.

Randall, G.E., 1989. Efficient calculation of differential seismograms for lithospheric receiver functions, *Geophys. J. Int.,* **99,** 469–481.

Rao, G.S.P. & Tewari, H.C., 2005. The seismic structure of the Saurashtra crust in northwest India and its relationship with the Réunion Plume, *Geophys. J. Int.,* **160,** 318–330.

Richards, M., Contreras-Reyes, E., Lithgow-Bertelloni, C., Ghiorso, M. & Stixrude, L., 2013. Petrological interpretation of deep crustal intrusive bodies beneath oceanic hotspot provinces, *Geochem. Geophys. Geosyst.,* **14,** 604–619.

Rychert, C.A. & Shearer, P.M., 2009. A global view of the lithosphere-asthenosphere boundary, *Science,* **324,** 495–498.

Sambridge, M.S., 1999a. Geophysical inversion with a neighbourhood algorithm. I. Searching a parameter space, *Geophys. J. Int.,* **138,** 479–494.

Sambridge, M.S., 1999b. Geophysical inversion with a neighbourhood algorithm – II. Appraising the ensemble, *Geophys. J. Int.,* **138,** 727–746.

Sambridge, M.S., 2001. Finding acceptable models in nonlinear inverse problems using a neighbourhood algorithm, *Inverse Problems,* **17,** 387–403.

Sambridge, M., Gallagher, K., Jackson, A. & Rickwood, P., 2006. Trans-dimensional inverse problems, model comparison and the evidence, *Geophys. J. Int.,* **167,** 528–542.

Savage, M.K., 1998. Lower crustal anisotropy or dipping boundaries? Effects on receiver functions and a case study in New Zealand, *J. geophys. Res.,* **103,** 15 069–15 087.

Sheehan, A.F., Abers, G.A., Jones, C.H. & Lerner-Lam, A.L., 1995. Crustal thickness variations across the Colorado Rocky Mountains from teleseismic receiver functions, *J. geophys. Res.,* **100,** 20 391–20 404.

Sheth, H.C., 1999. Flood basalts and large igneous provinces from deep mantle plumes: fact, fiction, and fallacy, *Tectonophysics,* **311,** 1–29.

Shibutani, T., Sambridge, M.S. & Kennett, B.L.N., 1996. Genetic algorithm inversion for receiver functions with application to crust and uppermost mantle structure beneath Eastern Australia, *Geophys. Res. Lett.,* **23,** 1826–1832.

Shor, Jr. G.G. & Pollard, D.D., 1963. Seismic Investigations of Seychelles and Saya de Malha Banks, Northwest Indian Ocean, *Science,* **142,** 48–49.
Smith, W.H.F. & Sandwell, D.T., 1997. Global sea floor topography from satellite altimetry and ship depth soundings, *Science,* **277,** 1956–1963.
Stutzmann, E., Roult, G. & Astiz, L., 2000. GEOSCOPE station noise levels, *Bull. seism. Soc. Am.,* **90,** 690–701.
Tan, B.H., Jackson, I. & Fitz Gerald, J.D., 1997. Shear wave dispersion and attenuation in fine-grained synthetic olivine aggregates: preliminary results, *Geophys. Res. Lett.,* **24,** 1055–1058.
Thomson, W.T., 1950. Transmission of elastic waves through a stratified solid, *J. appl. Phys.,* **21,** 89–93.
Thoraval, C., Tommasi, A. & Doin, M.-P., 2006. Plume-lithosphere interaction beneath a fast moving plate, *Geophys. Res. Lett.,* **33,** 1–4.
Tkalčić, H., Pasyanos, M.E., Rodgers, A.J., Gök, R., Walter, W.R. & Al-Amri, A., 2006. A multistep approach for joint modeling of surface wave dispersion and teleseismic receiver functions: implications for lithospheric structure of the Arabian Peninsula, *J. geophys. Res.,* **111,** B11311, doi:10.1029/2005JB004130.
Tkalčić, H., Chen, Y., Liu, R., Huang, H., Sun, L. & Chan, W., 2011. Multi-Step modelling of teleseismic receiver functions combined with constraints from seismic tomography: crustal structure beneath southeast China, *Geophys. J. Int.,* **187,** 303–326.
Tkalčić, H., Rawlinson, N., Arroucau, P., Kumar, A. & Kennett, B.L.N., 2012. Multistep modeling of receiver-based seismic and ambient noise data from WOMBAT array: crustal structure beneath southeast Australia, *Geophys. J. Int.,* **189,** 1681–1700.
Torsvik, T.H. *et al.*, 2013. A Precambrian microcontinent in the Indian Ocean, *Nat. Geosci.,* **6,** 223–227.
Vinnik, L., 1977. Detection of waves converted from P to SV in the mantle, *Phys. Earth planet. Inter.,* **15,** 39–45.
Voronoi, M.G., 1908. Nouvelles applications des paramètres continus à la théorie des formes quadratiques, *J. reine Angew. Math.,* **134,** 198–287.
Watts, A.B., ten Brink, U.S., Buhl, P. & Brocher, T.M., 1985. A multichannel seismic study of lithospheric flexure across the Hawaiian-Emperor seamount chain, *Nature,* **315,** 105–111.
Zelt, B.C. & Ellis, R.M., 1999. Receiver-function studies in the Trans-Hudson Orogen, Saskatchewan, *Can. J. Earth Sci.,* **36,** 585–603.
Zhu, L. & Kanamori, H., 2000. Moho depth variation in southern California from teleseismic receiver functions, *J. geophys. Res.,* **105,** 2969–2980.

SUPPORTING INFORMATION

Additional Supporting Information may be found in the online version of this paper:

Appendix A1: Example of individual radial RFs traces (black lines) we used for the stack (green line) at RER (a) and MRIV (b).
Appendix A2: Example of individual radial RFs traces (black lines) we used for the stack (green lines) at RODM (a), DGAR (b), KAAM (c) and HMDM (d).
Appendix B: Model parameter space bounds used in the NA receiver function inversion.
Appendix C: TB inversion.
Appendix D: *H*-κ stacking result at MRIV seismic station.
(http://gji.oxfordjournals.org/lookup/suppl/doi:10.1093/gji/ggv279/-/DC1).

Please note: Oxford University Press is not responsible for the content or functionality of any supporting materials supplied by the authors. Any queries (other than missing material) should be directed to the corresponding author for the paper.